International Journal of Nanomedicine

Dovepress
open access to scientific and medical research

Open Access Full Text Article

ORIGINAL RESEARCH

Surface modulation of single-walled carbon nanotubes for selective bacterial cell agglutination

This article was published in the following Dove Medical Press journal:
International Journal of Nanomedicine

Elena Romero-Ben[1]
Juan José Cid[1]
Mohyeddin Assali[1]
Elisabeth Fernández-García[2]
Ralf Erik Wellinger[2]
Noureddine Khiar[1]

[1]Asymmetric Synthesis and Functional Nanosystems Group, Institute of Chemical Research-Universidad de Sevilla, Avda. Américo Vespucio, 41092 Seville, Spain; [2]Genome Stability Department, Andalusian Center for Molecular Biology and Regenerative Medicine Centre, Universidad de Sevilla-CSIC, Avda. Américo Vespucio, 41092 Seville, Spain

Background: Bacterial resistance to antibiotics is one of the biggest challenges facing medicine today. Anti-adhesive therapy, using inhibitors of bacterial adhesion to epithelial cells, one of the first stages of infection, is a promising approximation in this area. The size, shape, number of sugar and their placement are variables that have to be taken into account in order to develop multivalent systems able to inhibit the bacterial adhesion based on sugar-lectin interaction.

Materials and methods: In the present work we report a modular approach for the synthesis of water-soluble 1D-carbon nanotube-sugar nanoconstructs, with the necessary flexibility to allow an efficient sugar-lectin interaction. The method is based on the reaction of aryl diazonium salts generated in situ from aniline-substituted mannose and lactose derivatives with single wall carbon nanotubes (SWCNTs) sidewalls.

Results: Two hybrid nanosystems, I-II, exposing mannose or lactose and having a tetraethylene glycol spacer between the sugar and the nanotube sidewall were rapidly assembled and adequately characterized. The sweet nano-objects were then tested for their ability to agglutinate and selectively inhibit the growth of uropathogenic *Escherichia coli*. These studies have shown that nanosystem I, exposing mannose on the nanotube surface is able to agglutinate and to inhibit the bacterial growth unlike nano-objects II exposing lactose.

Conclusion: The results reported constitute a proof of principle in using mannose-coated 1D-carbon nanotubes as antiadhesive drugs that compete for FimH binding and prevent the uropathogenic bacteria from adhering to the urothelial surface.

Keywords: single-walled carbon nanotubes, carbohydrates, bacterial resistance, antiadhesive therapy, multivalency, aryl diazonium salts chemistry

Introduction

Multivalent interactions are essential for achieving strong, yet reversible interactions in a large number of biologically relevant events.[1,2] Multivalency is especially prevalent in glycobiology, where effective interactions between lectins (carbohydrate-binding proteins) and their cognate carbohydrate ligands are achieved, despite the low affinity usually observed in the interaction of the said lectin with its monovalent epitope.[3–9] The relevance of these interactions in fertilization, immune response, cell adhesion, and tumor cell metastasis, among others, has put research on glycobiology in the frontline of pharmaceutical and medical research.[10–13] On the other hand, many infections by pathogens and toxins are also mediated by carbohydrate–lectin interactions.[14] In this sense, urinary tract infections (UTIs), which are among the most prevalent infectious diseases worldwide affecting millions of people every year, are mainly caused by uropathogenic strains of *Escherichia coli* (UPEC).[15] As it is the case for other diseases caused by bacteria, currently, antibiotics are the main treatment for acute uncomplicated lower UTIs. However, the repeated and misuse of antibiotics has led to increased

Correspondence: Noureddine Khiar
Asymmetric Synthesis and Functional Nanosystems Group, Instituto de Investigaciones Químicas CSIC-Universidad de Sevilla, Avda. Américo Vespucio, 49, 41092 Seville, Spain
Tel +34 95 448 9559
Fax +34 95 446 0565
Email khiar@iiq.csic.es

submit your manuscript | www.dovepress.com
Dovepress
http://dx.doi.org/10.2147/IJN.S179202

antibacterial resistance,[16] and the possible looming of a post-antibiotic era, highlighting the need for new strategies for the prevention and treatment of microbial infections.[17–20] In the particular case of UTIs, adherence to the urothelial surface, one of the early stages of the infection, is mediated by the mannose-specific lectin FimH located at the tip of bacterial type 1 pili.[21] The FimH lectin was identified as an attractive target for an alternative way of preventing and treating UTIs by using mannose-based antagonists as antiadhesive drugs that compete for FimH binding with mannose residues on high mannose N-glycans of the transmembrane glycoprotein uroplakin Ia.[22] By blocking the adhesin, FimH antagonists prevent UPEC from adhering to the urothelial surface and avert every subsequent step of the infection cycle, including bacterial invasion of host cells and formation of biofilms. A substantial advantage of this antiadhesive approach over conventional antibiotic treatment is the reduced risk of resistance development, as FimH antagonists do not exert selection pressure on uropathogens.[23] Even assuming that this would be the case, the bacteria would possibly lose their ability to adhere to the cell surface and therefore, their virulence. Over the past decades, efforts in developing potent FimH antagonists as antiadhesive drugs for the treatment of UTIs have led to various synthetic multivalent surrogates, designed to take advantages of the so-called "cluster glycoside effect".[24] Given the accessibility and facility in functionalizing scaffolds such as metal nanoparticles, dendrimers, calixarenes, fullerenes, and cyclodextrins, the majority of the multivalent systems obtained so far have spherical shapes.[25,26] Recent studies have shown that the geometry of glycocoated nanosystems has a significant impact on their abilities to generate networks and to interact with specific lectins present in biological membranes. In this sense, it has recently been reported that whereas spherical mannose-coated micelles are inhibitors of a globular lectin, concanavalin A, the mannose-coated one-dimensional (1D) cylindrical nanosystems are more suited for the inhibition of bacterial motility.[27–30] Thus, the synthesis of multivalent 1D glyconanomaterial, ideally endowed with the desired adaptability and flexibility needed to optimize protein–carbohydrate interactions at the fluid and dynamic interface of the cell surface, are of great importance in glycobiology.

One-dimensional carbon nanotubes hold unique structural, mechanical, electrical, and optical properties for their application in glycobiology and in other biomedical applications.[31,32] Based on these premises, we have recently reported various bottom-up approaches for the synthesis of sugar-coated carbon nanotubes, based on hydrophobic or π–π interactions between well-designed neoglycolipids and sidewall of single-walled carbon nanotubes (SWCNTs).[33–36] Here, we report the covalent functionalization of SWCNTs with aniline-substituted mannose and lactose derivatives (Figure 1) by means of the radical addition of their aryl diazonium species thermally generated in situ. The radical addition of aryl diazonium salts, generated upon electrochemical or thermal treatment, has shown to be a powerful tool by itself for the functionalization, solubilization, and dispersion of SWCNTs.[37–39] In our examples, this reaction

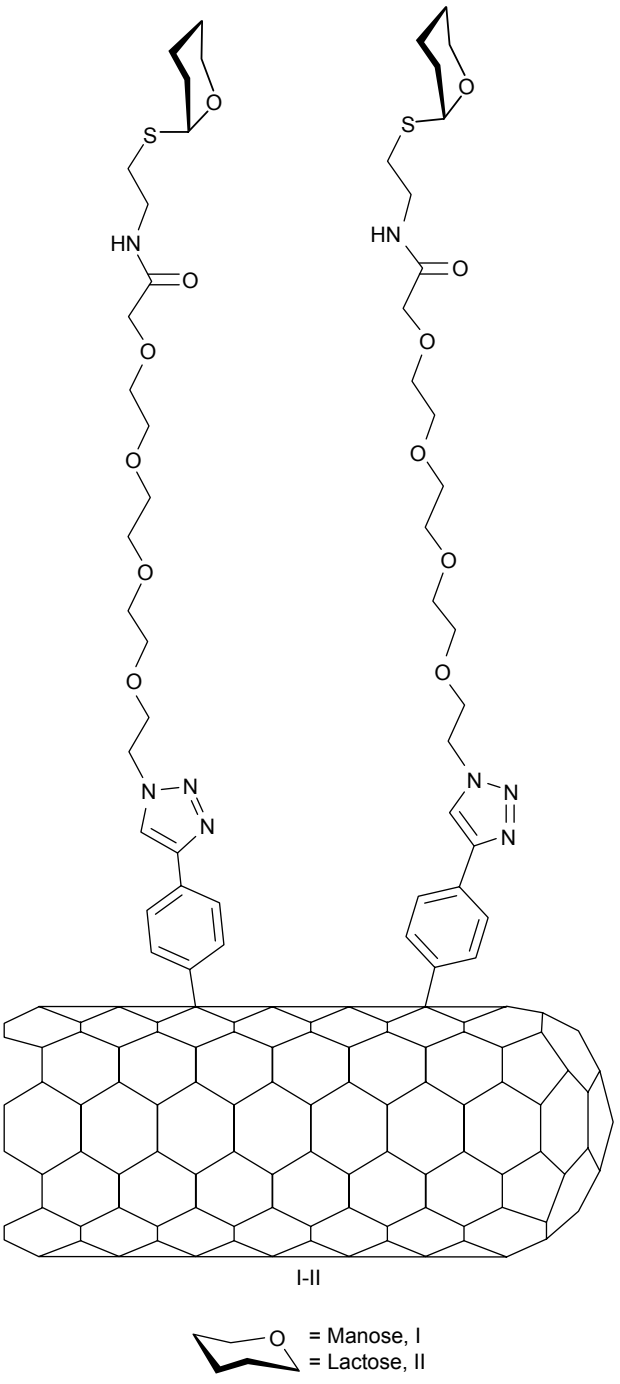

Figure 1 General structure of the glyconanotube used in this study.

has shown to be an easy-to-perform and efficient approximation to afford the highly functionalized water-soluble carbon derivatives with a spacer between the sugar head group and the SWCNT sidewall designed to optimize the interactions of the sugar epitopes and their cognate receptors.

The structures of the 1D nanomaterials produced have been investigated by nuclear magnetic resonance (NMR), transmission electronic microscopy (TEM), scanning transmission electronic microscopy (STEM), scanning electronic microscopy (SEM), and Raman and ultraviolet/visible/near infrared (UV/Vis/NIR) spectroscopies. The sugar content in the 1D nanoconstructs has been determined by thermogravimetric analysis (TGA). Finally, we determined the potency and selectivity of these nanomaterials to aggregate the enterobacteria *E. coli* type 1 fimbriae, through their interactions with mannose-specific lectin FimH located at the tip of bacterial pili. The results reported constitute a proof of principle in using mannose-coated 1D carbon nanotubes as antiadhesive drugs that compete for FimH binding and prevent the uropathogenic bacteria from adhering to the urothelial surface.

Materials and methods

Chemicals employed for all the experiments in this study were purchased from Aldrich Chemical Co., Inc and Carbosynth Co., Inc. SWCNTs were obtained commercially from Carbon Solutions Co., Ltd and used as received without further purification. Dry solvents were purchased from SDS in anhydrous grade and in addition dried in a solvent purification system (Pure Solv MD5, Innovative Technology). The monitoring of the reactions was carried out by thin layer chromatography, employing aluminum sheets coated with silica gel 60 F_{254} (normal phase) purchased from Merk. Sonications were accomplished by using a sonication tip (Qsonica Ultrasonic Liquid Processor, Q500 model) and a water bath (Ultrasonik®, ULTRAsonik NEY 28B bath, Cleaning Technolgies Group. Cincinnati, OH, USA). TGA were carried out with TA Instruments (TGA Q600 thermal analyzer) in the temperature range of 0°C–600°C, with a heating rate of 20°C/min and under N_2 (100 mL/min). Raman spectra were recorded on a LabRAM HR800 high-resolution UV confocal Raman microscope using a red laser (He–Ne 785 nm), 600 line/mm, 20× objective, 20 mW, and 100 µm pinhole. NMR spectra were recorded with a Bruker AC-400 and a Bruker AC-500 apparatus (Figures S1–S4). Deuterated solvents are indicated in brackets. Chemical shift values (δ) are referred to tetramethylsilane, utilized as internal reference; then, the spectral signals were calibrated according to the nondeuterated residual peak of the solvent. Optical rotations $[\alpha]^{20}_{D}$ were determined with a Perkin-Elmer 341 polarimeter using a sodium lamp (λ=589 nm) with a 10 cm cell length. UV/Vis/NIR spectra were recorded in dispersions using Milli-Q water or dimethylformamide (DMF) purchased from Fluka Chemie in spectroscopic grade on a UV/vis Perkin-Elmer Lambda 12, using quartz cuvettes. High-resolution mass spectrometry (HR-MS) were recorded on a Kratos MS-80RFA 241-MC apparatus. TEM images were taken using Philips CM 200 with an accelerating voltage of 200 kV. SEM and STEM images were taken using emission scanning microscope (field-emission SEM [FESEM], Schottky type) with an STEM detector having eight individual channels that allow transmission images to be captured in brightfield, darkfield, and high-angle darkfield illuminations.

Synthesis of amino-substituted sugars **11** and **12**

Synthesis of compound **2**

A mixture of 4-ethynylaniline **1** (747 mg, 6.38 mmol) and di-*tert*-butyl dicarbonate (5.26 mL, 22.9 mmol) in tetrahydrofuran (THF) (6.5 mL) was stirred at room temperature for 3 hours. Then, the reaction mixture was evaporated to obtain the crude product, which was purified by column chromatography (hexane/AcOEt 15:1), affording the title compound **2** as a yellow solid (748 mg, 3.45 mmol, 54%). Mp: 98.2°C–99.3°C. R_f: 0.42 (CH_2Cl_2/MeOH 15:1). ^{1}H NMR (500 MHz, $CDCl_3$): δ 7.43 (d, 2H, J = 1.9 Hz, Ar), 7.35 (d, 2H, J = 1.9 Hz, Ar), 6.82 (s, 1H, NH), 3.05 (s, 1H, CC–H), 1.52 (s, 9H, $C(CH_3)_3$). ^{13}C NMR (125.7 MHz, $CDCl_3$): δ 152.5 (CO), 139.0 (Ar), 132.9 (Ar), 118.1 (Ar), 116.3 (Ar), 83.6 (Ar<u>C</u>CH), 80.9 (ArC<u>C</u>H), 76.5 ($\underline{C}CH_3)_3$, 28.3 ($C(\underline{C}H_3)_3$). HRMS Calcd for $C_{13}H_{15}NO_2Na$ 240.1103 [M+Na]+, found a 240.0998.

Synthesis of compound **7**

To a solution of copper sulfate (3.2 mg, 0.02 mmol) and sodium L-ascorbate (11.33 mg, 0.061 mmol) in distilled water (1.39 mL), was added a solution of azide compound **5** (90 mg, 0.135 mmol) and alkyne **2** (35.2 mg, 0.162 mmol) in CH_2Cl_2 (1.36 mL). The reaction mixture was stirred for 20 minutes in a microwave apparatus at 110°C. The solvent was evaporated and the crude product was purified by column chromatography (CH_2Cl_2/MeOH, 40:1), affording regioselectively the 1,4-disubsituted triazol **7** as a light brown syrup with a 62% yield (88.7 mg, 0.1 mmol). R_f: 0.37 (CH_2Cl_2/ MeOH 15:1). $[\alpha]_D^{20}$: +19.8 (c. 1, $CHCl_3$). ^{1}H NMR (400 MHz, $CDCl_3$): δ 8.00 (s, 1H, Triazol), 7.79 (d, 2H, J = 5 Hz, Ar), 7.46 (d, 2H, J = 6.19 Hz, Ar), 7.31 (t, 1H, J = 6 Hz, NHCO), 6.75 (s, 1H, NHBoc), 5.35–5.29 (m, 3H, H-4, H-1, H-2), 5.24 (dd, $J_{3,4}$ = 10 Hz, $J_{3,2}$ = 3.2 Hz,

1H, H-3), 4.60 (t, J = 4.7 Hz, 2H, CH_2N-Triazol), 4.40–4.37 (m, 1H, H-5), 4.34–4.30 (dd, 1H, $J_{6a,6b}$ = 12 Hz, $J_{6a,5}$ = 5.4 Hz, H-6a), 4.13–4.10 (dd, 1H, $J_{6b,6a}$ = 12 Hz, $J_{6b,5}$ = 2 Hz, H-6b), 3.99 (s, 2H, $COCH_2O$), 3.93 (t, J = 4.8 Hz, 2H, OCH_2CH_2N-Triazol), 3.64–3.61 (m, 12H, $6CH_2O$), 3.55-3.51 (m, 2H, CH_2NH), 2.86-2.75 (m, 2H, $-SCH_2$), 2.17 (s, 3H, CH_3COO), 2.10 (s, 3H, CH_3COO), 2.06 (s, 3H, CH_3COO), 2.00 (s, 3H, CH_3COO), 1.54 (s, 9H, Boc). ^{13}C NMR (125.7 MHz, CDCl3): δ 170.64 (CO), 170.21 (CO), 169.97 (CO), 169.88 (CO), 169.70 (CO), 152.68 (C-Triazol), 138.37, 126.33 (C-Ar), 125.57 (C-triazol), 118.68 (C-Ar), 82.47, 80.6 (C-1), 77.37, 77.06, 76.74 (C-5), 70.90 (C2), 70.60, 70.47, 70.38, 70.25 (CH_2O, CH_2-CH_2-triazol), 69.48, 69.43, 69.16 (C-3), 66.21 (C-4), 62.41 (C-6), 50.45 (CH_2-Triazol), 38.12 (CH_2NH), 31.10 (SCH_2), 28.35 (Boc), 20.90 (CH_3), 20.70 (CH_3), 20.70 ($2CH_3$), 20.64 (CH_3). HRMS Calcd for $C_{39}H_{57}O_{16}N_5S$ 884.3594 [M+H]+, found 884.3594.

Synthesis of compound **9**

To a solution of mannoside **7** (420 mg, 0.47 mmol) in 4 mL of CH_2Cl_2 under argon atmosphere, trifluoroacetic acid was added at 0°C (0.72 mL, 9.4 mmol). The reaction mixture was monitored by TLC plate, and more equivalents of trifluoroacetic acid (TFA) were added until the reaction was complete. The solvent was evaporated, and the crude product purified by flash column chromatography (CH_2Cl_2/MeOH, 20:1), to give the title compound **9** as a light brown solid with a 99% yield (370 mg, 0.47 mmol). Mp: 60.1°C–63.9°C. R_f: 0.12 (CH_2Cl_2/MeOH 15:1). $[\alpha]_D^{20}$: +34.5 (c 1.0, $CHCl_3$). ^{1}H NMR (400 MHz, $CDCl_3$): δ 7.29 (s, 1H, Triazol), 7.67 (d, J = 7.9 Hz, 2H, Ar), 7.44 (s, 1H, NH), 6.91 (d, J = 7.7 Hz, 2H, Ar), 5.35–5.31 (m, 3H, H-4, H-1, H-2), 5.25 (dd, $J_{3,4}$ = 10 Hz, $J_{3,2}$ = 3.2 Hz, 1H, H-3), 4.63–4.60 (t, J = 4.7 Hz, 2H, CH_2N-triazol), 4.40–4.36 (m, 1H, H-5), 4.34–4.30 (dd, 1H, $J_{6a,6b}$ = 12 Hz, $J_{6a,5}$ = 5.2 Hz, H-6a) 4.15–4.12 (dd, 1H, $J_{6b,6a}$ = 12 Hz $J_{6b,5}$ = 2 Hz, H-6b), 4.00 (s, 2H, $-COCH_2O$), 3.96 (t, J = 4.5 Hz, 2H, $-OCH_2CH_2$N-triazol), 3.66-3.62 (m, 12H, $6CH_2O$), 3.56-3.53 (m, 2H, CH_2NH), 2.98 (s, 2H, NH_2), 2.87-2.75 (m, 2H, $-SCH_2$), 2.18 (s, 3H, CH_3COO), 2.11 (s, 3H, CH_3COO), 2.08 (s, 3H, CH_3COO), 2.01 (s, 3H, CH_3COO). ^{13}C NMR (100 MHz, $CDCl_3$): δ 170.7 (CO), 170.1 (CO), 169.1 (CO), 169.7 (2 CO), 146.8 (C-triazol), 137.9 (Ar), 126.9 (C-triazol), 126.3 (C-triazol), 121.0 (Ar), 119.9 (Ar), 82.3 (C-1), 77.4, 77.1, 76.7 (C-5), 70.9 (C-2), 70.8 (C-3), 70.5, 70.3, 70.2, 70.1, 69.5 (CH_2O, CH_2-CH_2-triazol), 66.2 (C-4), 62.4 (C-6), 50.3 (CH_2N-triazol), 38.2 (CH_2NH), 30.9 (SCH_2), 20.8 (CH_3), 20.6 (2 CH_3), 20.6 (CH_3). HRMS Calcd for $C_{34}H_{49}N_5O_{14}SNa$ 806.2889 [M+Na]+, found 806.2872.

Synthesis of compound **11**

To a solution of **9** (150 mg, 0.19 mmol) in 3 mL of dry methanol under argon atmosphere was added a solution of freshly prepared 1M MeONa in MeOH (0.1 eq for each acetate). The reaction mixture was stirred for 1 hour, and then neutralized with acidic resin, Amberlite® IR 120 H^+, Fluka (Merck Group, Darmstadt, Germany). The reaction mixture was filtered over a pad of celite, and then the solvent was evaporated under reduced pressure to give the ammonium salt of the desired compound (116 mg, 0.16 mmol). The neutral amine **11** (93 mg, 0.15 mmol, 80%) was obtained as a yellow-brown syrup by using ion exchange chromatography (Isolute SPESCX-2). R_f: 0 (CH_2Cl_2/MeOH 9:1). $[\alpha]^{20}$ D: +40,8 (c 0.5, MeOH). ^{1}H NMR (400 MHz, MeOD): δ 8.19 (s, 1H, Triazol), 7.57 (d, 2H, J = 8.38 Hz, Ar), 6.70 (d, 2H, J = 8.35 Hz, Ar), 5.30 (s, 1H, H-1), 4.63 (t, 2H, J = CH_2-Triazol), 3.97 (s, 2H, $COCH_2O$), 3.95–3.87 (m, 5H, H-4, H-2, H-6a, CH_2-CH_2-triazol), 3.77–3.72 (dd, 1H, $J_{6b,6a}$ = 12 Hz, $J_{6b,5}$ = 6.2 Hz, H-6b), 3.66–3.59 (m, 16H, $6CH_2O$, NH_2, H-3, H-5), 3.56-3.44 (m, 2H, CH_2NH), 2.89–2.69 (m, 2H, SCH_2).^{13}C NMR (125.7 MHz, MeOD): δ 162.30, 161.95, 161.61, 161.26 (CO), 148.01 (C-Triazol), 126.42 (C-Ar), 120.21, 119.77, 118.22 (C-triazol), 115.10 (C-Ar), 85.16 (C-1), 73.77 (C-4), 72.24 (C-2), 71.72 (C-3), 70.24, 70.08, 69.85, 69.78, 69.54 (CH_2O, CH_2-CH_2-triazol), 69.13 (C-5), 61.33 (C-6), 49.98 (CH_2-Triazol), 38.38 (CH_2NH), 30.08 (SCH_2). HRMS Calcd for $C_{26}H_{42}O_{10}N_5S$ 615.2647 [M+H]+, found 615.2639.

Synthesis of compound **8**

To a solution of copper sulfate ($CuSO_4$) (2.9 mg, 0.0185 mmol) and sodium L-ascorbate (10.9 mg, 0.0553 mmol) in distilled water (1.39 mL) was added a solution of azide compound **6** (126 mg, 0.132 mmol) and alkyne **2** (34 mg, 0.16 mmol) in CH_2Cl_2 (1.36 mL). The reaction mixture was stirred at 110°C for 20 minutes. The solvent was evaporated and the crude reaction mixture was purified by column chromatography (CH_2Cl_2/MeOH, 40:1), affording the title compound **8** as a brown solid with 80% yield (123.8 mg, 0.11 mmol). Mp: 77.2°C–79.9°C. R_f: 0.28 (CH_2Cl_2/MeOH 15:1). $[\alpha]_D^{20}$: −5 (c 1.0, $CHCl_3$). ^{1}H NMR (400 MHz, $CDCl_3$): δ 7.95 (s, 1H, triazol), 7.78 (d, 2H, J = 8.6 Hz, Ar), 7.45 (d, 2H, J = 8.6 Hz, Ar), 7.25 (t, 1H, J = 5.8 Hz, NHCO), 6.75 (s, 1H, NHBoc), 5.36 (d, 1H, $J_{4',3'}$ = 2.4 Hz, H-4′), 5.20 (t, 1H, $J_{2,3}$ = $J_{3,4}$ = 9.5 Hz, H-3), 5.11 (dd, 1H, $J_{2',3'}$ = 10.0 Hz, $J_{2',1'}$ = 8.0 Hz, H-2′), 4.97 (t, 1H, $J_{3',4'}$ = 3.4 Hz, $J_{3,2'}$ = 10 Hz, H-3′), 4.92 (t, 1H, $J_{3,4}$ = $J_{3,2}$ = 9.8 Hz, H-3), 4.60 (t, 2H, J = 4.8, CH_2-triazol), 4.54-4.49 (m, 3H, H-1, H-1′, H-6a), 4.16-4.05 (m, 3H, H-6b, H-6′), 3.97 (s, 2H, $COCH_2O$), 3.94-3.88 (m,

3H, H-5′, C<u>H</u>$_2$-CH$_2$-triazol), 3.79 (t, 1H, $J_{4,3} = J_{4,5} = 9.5$ Hz, H-4), 3.64-3.61 (m, 13H, 6 CH$_2$O, H-5), 3.60-3.46 (m, 2H, CH$_2$NH), 2.88-2.73 (m, 2H, SCH$_2$), 2.17 (s, 3H, CH$_3$COO), 2.16 (s, 3H, CH$_3$COO), 2.12 (s, 3H, CH$_3$COO), 2.09 (s, 3H, CH$_3$COO), 2.06 (s, 6H, 2 CH$_3$COO), 1.97 (s, 3H, CH$_3$COO), 1.54 (s, 9H, Boc). ^{13}C NMR (125.7 MHz, CDCl$_3$): δ 170.4 (CO), 170.3 (CO), 170.2 (CO), 170.1 (CO), 170.0 (CO), 169.7 (CO), 169.6 (CO), 169.1 (CO), 152.6, 147.3 (C-triazol), 138.3, 126.3, 125.4 (C-Ar), 120.5 (C-triazol), 118.7 (C-Ar), 101.0 (C-1′), 83.6 (C-1), 80.6, 77.3, 77.1, 76.7 (C-5), 76.1 (C-4), 73.7 (C-3), 71.0 (C-3′), 70.9 (C-5′), 70.7–70.2 (CH$_2$O, CH$_2$CH$_2$-triazol), 69.5 (C-2′), 69.1 (C-2), 66.6 (C-4′), 62.1 (C-6), 60.7 (C-6′), 53.4, 50.3 (CH$_2$-triazol), 38.9 (CH$_2$NH), 30.9, 30.4, 29.7 (SCH$_2$), 28.3 (Boc), 20.8 (CH$_3$), 20.7 (CH$_3$), 20.6 (CH$_3$), 20.5 (CH$_3$), 20.6 (CH$_3$). HRMS Calcd for $C_{51}H_{73}O_{24}N_5NaS$ 1194.4245 [M+Na]+, found 1,194.4258.

Synthesis of compound **10**

To a solution of lactoside **8** (495 mg, 0.422 mmol) in 4 mL of CH$_2$Cl$_2$ under argon atmosphere was added trifluoroacetic acid at 0°C (0.65 mL, 8.45 mmol). The reaction mixture was monitored by TLC plate, and more equivalents of TFA were added until the reaction was complete. The product was purified by flash chromatography (CH$_2$Cl$_2$/MeOH, 20:1), to give the title compound **10** as a dark yellow syrup with an 80% yield (360 mg, 0.34 mmol). R$_f$: 0.13 (CH$_2$Cl$_2$/ MeOH 15:1). $[\alpha]_D^{20}$: –5,69 (c 0.72, CHCl$_3$). ^{1}H NMR (400 MHz, CDCl$_3$): δ 8.09 (s, 1H, triazol), 7.67 (d, 2H, J = 8.6 Hz, Ar), 7.49 (t, 1H, J = 5.8 Hz, NHCO), 7.37 (d, 2H, J = 8.6 Hz, Ar), 5.40 (d, 1H, $J_{4',3'} = 2.4$ Hz, H-4′), 5.20 (t, 1H, $J_{3,4} = J_{3,2} = 9.5$ Hz, H-3), 5.11 (dd, 1H, $J_{2',3'} = 10.0$ Hz, $J_{2',1'} = 8.0$ Hz, H-2′), 5.03, (dd, 1H, $J_{3',2'} = 10.4$, $J_{3',4'} = 3.3$ Hz, H-3′), 4.94 (t, 1H, $J_{2,3} = J_{2,1} = 9.7$ Hz, H-2), 4.67 (t, 2H, J = 3.7 Hz, CH$_2$-Triazol), 4.60 (dd, 1H, $J_{6a,6b} = 10.9$ Hz, H6a), 4.54 (d, 1H, $J_{1',2'} = 8$ Hz, H-1′), 4.50 (d, 1H, $J_{1,2} = 10$ Hz, H-1), 4.20-4.09 (m, 5H, H-6b, H-6′a, H-6′b, NH$_2$), 3.98 (s, 2H, COCH$_2$O), 3.96-3.92 (t, 1H, $J_{5',4'} = J_{5',6'} = 6.8$ Hz, H-5′), 3.81 (m, 3H, O<u>CH</u>$_2$CH$_2$-triazol, H-4), 3.79-3.64 (m, 13H, 6 CH$_2$O, H-5), 3.55-3.52 (m, 2H, CH$_2$NH), 2.87-2.69 (m, 2H, SCH$_2$), 2.19 (s, 3H, CH$_3$COO), 2.12 (s, 3H, CH$_3$COO), 2.10 (s, 3H, CH$_3$COO), 2.10 (s, 3H, CH$_3$COO), 2.09 (s, 6H, CH$_3$COO), 2.07 (s, 3H, CH$_3$COO), 2.01 (s, 3H, CH$_3$COO). ^{13}C NMR (125.7 MHz, CDCl$_3$): δ 208.1, 171.6 (CO), 170.8 (CO), 170.5 (CO), 170.25 (CO), 170.18 (CO), 170.0 (CO), 169.95 (CO), 169.42 (CO) 145.6 (C-triazol), 131.24, 129.8 (C-Ar), 127.3, 123.3 (C-Ar), 122.3 (C-triazol), 100.9 (C-1′), 83.6 (C1), 77.3, 77.1, 76.74 (C-5), 75.8 (C-4), 73.6 (C-3), 70.9 (C-3′), 70.7 (C-5′), 70.3–70.0 (CH$_2$O, C<u>H</u>$_2$-CH$_2$-C-triazol), 69.6 (COCH$_2$O), 69.2 (C-2′), 68.9 (C-2), 66.7 (C-4′), 61.9 (C-6′), 60.8 (C-6), 50.3 (CH$_2$-triazol), 39.3 (CH$_2$NH), 30.9 (SCH$_2$), 20.8 (CH$_3$), 20.7 (CH$_3$), 20.6 (CH$_3$), 20.6 (2 CH$_3$), 20.5 (CH$_3$), 20.5 (CH$_3$). HRMS Calcd for $C_{46}H_{65}O_{22}N_5SNa$ 1,094.3734 [M+Na]+, found 1,094.3750.

Synthesis of compound **12**

To a solution of **10** (170 mg, 0.16 mmol) in 3 mL of dry methanol under argon atmosphere was added a solution of freshly prepared 1M MeONa in MeOH (0.1 eq for each acetate). The reaction mixture was stirred for 1 hour, and then neutralized with acidic resin, Amberlite® IR 120 H$^+$. The reaction mixture was filtered over a pad of celite, and then the solvent was evaporated under reduced pressure to give the ammonium salt of the desired compound (125 mg, 0.16 mmol). The free amine **12** (100 mg, 0.12 mmol, 75%) was obtained as a brown syrup by using ion exchange chromatography (Isolute SPESCX-2). R$_f$: 0 (CH$_2$Cl$_2$/MeOH 9:1). $[\alpha]_D^{20}$: –6.31 (c 0.25, MeOH). ^{1}H NMR (400 MHz, MeOD): δ 8.19 (s, 1H, Triazol), 7.57 (d, 2H, J = 8.7 Hz, Ar), 6.79 (d, 2H, J = 8.7 Hz, Ar), 4.62 (t, 2H, J = 5 Hz, CH$_2$-Triazol), 4.45 (d, 1H, $J_{1,2} = 9.7$ Hz, H-1), 4.38 (d, 1H, $J_{1',2'} = 7.6$ Hz, H-1′), 3.97 (s, 2H, COCH$_2$O) 3.95-3.91 (m, 3H, H-6a, CH$_2$CH$_2$-triazol), 3.86–3.78 (m, 3H, H-6b, H-6′a, H-4′), 3.72 (dd, 1H, $J_{6'b,5'} = 4.6$ Hz, $J_{6'b,6'a} = 11.4$ Hz, H-6′b), 3.67-3.63 (m, 3H, H-5′, H-4, H-5), 3.63-3.48 (m, 17H, 6CH$_2$O, H-3, H-3′, H-2′, NH$_2$), 3.47–3.43 (m, 2H, C<u>H</u>$_2$NH), 3.31–3.28 (m, 1H, H-2), 2.92-2.76 (m, 2H, SCH$_2$). ^{13}C NMR (125.7 MHz, MeOD): δ 171.47 (CO), 147.97 (C-Triazol), 126.41 (C-Ar), 120.23 (C-triazol), 115.09 (C-Ar), 103.68 (C-1′), 85.61 (C1), 79.18, 79.01 (C-3), 76.5 (C3′), 75.7 (C-5), 73.43 (C-2′), 72.72 (C-2), 71.13 (C-5′), 70.52 (C-4), 70.2–69.8 (CH$_2$O, CH$_2$CH$_2$-triazol), 69.0 (COCH$_2$O), 68.9 (C-4′) 61.10 (C-6), 60.71 (C-6′), 50.09 (CH$_2$-Triazol), 39.09 (CH$_2$NH), 29.12 (SCH$_2$). HRMS Calcd for $C_{32}H_{52}O_{15}N_5S$ 778.3171 [M+H]+, found 778.3175. $[\alpha]_D^{20}$: –6.31 (c 0.25, MeOH).

Synthesis of functionalized SWCNTs I, II

General procedure: Pristine P2-SWCNTs (50 mg) and sugar 11 or 12 (~150 mg) were dried by making several "vac-refill" cycles in a Schlenk line and then dispersed in a (2:1) mixture (45 mL) of freshly distilled oDCB (orthodichlorobenzene) and DMF using an ultrasonication tip (15-minute cycle, 5 seconds On, 5 seconds Off, 30% amplitude) and cooling bath. The resulting black suspension was further sonicated in water bath (15 minutes) at room temperature while passing argon current. Then, isoamyl

nitrite (0.46 mL, 3.39 mmol) was added dropwise while stirring vigorously, and the reaction mixture was heated at 65°C for 24 hours under an argon atmosphere. After cooling to room temperature, the DMF was eliminated in vacuum and the afforded suspension filtered over a polytetrafluoroethylene (PTFE) (0.45 µm, Omnipore JHWP; EMD Millipore) membrane. The solid recovered on the filter was dispersed in methanol (300 mL), sonicated for 10 minutes in a water bath, and filtered over another PTFE (0.45 µm) membrane. The washing process was repeated in acetone (300 mL) and Et2O (300 mL). In order to remove the unfunctionalized or low functionalized SWCNTs, the collected black solid was suspended in Milli-Q water (100 mL) for 10 minutes. The black supernatant was decanted and concentrated in a rotary evaporator to yield, after drying in vacuum, ~61 mg of a black and lamellar solid. Finally, to eliminate any waste that could act like a toxin, the final nanosystems I and II were dialyzed in milli-Q water for a week.

Agglutination studies

The agglutination studies were carried out as described by Cid et al.[30] *E. coli* bacteria (ORN178 and ORN208 strains) were grown overnight at 37°C in Luria–Bertani (LB) medium with ampicillin in order to attain an OD measured at 600 nm (OD600) of ~1.0. The culture was centrifuged at 4,500 rpm for 5 minutes. The supernatant was discarded and the pellet was suspended in Milli-Q water. Aliquots of bacterial cells (100 µL) were mixed with nanosystem I (35 µL, 3 mg/mL) or nanosystem II (35 µL, 2.55 mg/mL). Finally, the mixture was incubated at 4°C for 30 minutes with gentle shaking to avoid bacterial cell division during incubation. Several preliminary tests have been carried out to determine the optimum selectivity conditions, which are those conditions that allow the maximum aggregation of the ORN178 bacteria, without affecting the ORN208 strains. After incubation, the mixture was centrifuged at 11,000 rpm for 5 minutes. The supernatant was discarded and the pellet was suspended, fixed in 2.5% formaldehyde, and observed under a wide-field fluorescence microscope (DM-6000B; Leica Microsystems) using N3 filter and a digital charge-coupled device camera (DFC350; Leica Microsystems). Pictures were processed using LAS AF software (Leica Microsystems). Approximately, 200 cells from three independent experiments were analyzed for each strain.

Colony forming assay

The colony forming assay was carried out as described by Cid et al.[30] *E. coli* bacteria (ORN178 and ORN208 strains) were grown overnight at 37°C in LB medium with ampicillin in order to obtain an OD measured at 600 nm (OD600) of ~5.0. The culture was centrifuged at 4,500 rpm for 5 minutes. The supernatant was discarded and the pellet was suspended in 700 µL of Milli-Q water. Aliquots of diluted bacterial cells (100 µL) were mixed with the nanosystem I (35 µL, 3 mg/mL) or nanosystem II (35 µL, 2.55 mg/mL). Finally, the mixture was incubated at 4°C for 30 minutes with shaking to avoid bacterial cell division during incubation. After incubation, the mixture was centrifuged at 1,500 rpm for 1.5 minutes. The pellet was discarded and the supernatant was diluted by 100,000 fold for evaluation. Petri dish plates were then incubated for 24 hours at 37°C, and the total number of colony-forming units (CFUs) was counted.

TEM analysis of bacterial cell agglutination

After incubation of the nanosystems with *E. coli* for 30 minutes, the aggregates were fixed by 2.5% formaldehyde (0.1M in PBS, pH 6.4) treatment and washed with PBS at pH 6.6 and 7.4. About 10 µL of the solution was then deposited on a copper grid coated with a carbon film, excess liquid was removed by filter paper, and then submerged in 2% uranyl acetate solution. TEM images were obtained using Philips CM200 apparatus with an accelerating voltage of 200 kV in Centro de Investigaciones Tecnológica e Innovación de la Universidad de Sevilla.

SEM analysis of bacterial cell agglutination

The samples of bacteria with functionalized SWCNTs were diluted in distilled water and deposited on a silicon wafer (10 µL), and the excess liquid was removed by a filter paper. After drying, the samples were coated with gold by ion sputtering deposition in a Leica EM SCD500 metalizer (10 nm), for its subsequent visualization in the FESEM (Schottky type) in Centro de Investigaciones Tecnológica e Innovación de la Universidad de Sevilla.

STEM analysis of bacterial cell agglutination

The visualization of the bacteria with functionalized SWCNT samples by STEM was carried out using the FESEM with a specific STEM detector and following the same methodology as for TEM analysis.

Results and discussion

One of the significant drawbacks that have limited the use of carbon nanotubes in biology is their high insolubility in water and their tendency to form dense ropes by interconnected tubes in a three-dimensional network. Currently, there are

several covalent,[40,41] noncovalent,[42–44] and hybrid[36] methods for the dispersion of carbon nanotubes in water, which have, among other, positive features to mitigate the cytotoxicity of pristine carbon nanotubes.[45] However, water solubility is not the only requirement for a biomaterial based on a carbon nanotube to be biocompatible and used in biological and biomedical processes. For this, it is necessary, in addition, to provide the hybrid nanomaterial with the possibility to escape the immune system and the ability to establish specific interactions with living cells. Most of these conditions are satisfied with the use of glyconanotubes, as carbohydrates are highly hydrophilic water-soluble molecules, capable of interacting with their specific receptors, and their anti-fouling capacity, similar to the widely used PEG, has been reported. Additionally, flexibility and adaptability are important for a multivalent biomaterial in order to establish efficient interactions with biological receptors located in the fluid and dynamic surface of the cells. Although the mechanic features of the nanotubes solve the problem of flexibility, the proper positioning of the sugars on the surface of the tube for optimal adaptability is very difficult to achieve.

Synthesis of the glyconanotubes

Considering this, we have decided to study the effect of a hydrophilic spacer placed between the saccharide head group and the nanotube sidewall in order to modulate the degree of freedom of the addendum and improve its adaptability. The designed compounds were mannose (I) and lactose (II) derivatives, separated by a spacer derived from tetraethyleneglycol (Figure 1). Based on their known glycosidase resistance, together with the similarity of their biological activity with the natural O-glycosides, we have worked with thioglycoside derivatives. For the synthesis of the desired aniline derivatives, the advanced azido derivatives 5 and 6, obtained in two-step process starting from the peracetylated starting sugars 3 and 4, have been used (Figure 2).[36]

The Cu(I)-catalyzed azido alkyne cycloaddition between the azido intermediate 5 and 4-ethynylaniline 1 failed to give the desired product.[46] However, the click reaction of both 5 and 6 and the Boc-derivative 2, using $CuSO_4$ in the presence of sodium ascorbate in a mixture of methylene chloride water, afforded regioselectively the 1,2,3–triazole derivatives 7 and 8 in 62% and 80% yields, respectively. Desprotection of the Boc group with trifluoroacetic acid afforded the ammonium salt derivatives 9 and 10 in 99% and 80% yields, respectively. Finally, a Zemplen desprotection[47] of the acetate yielded using sodium methylate in methanol, followed by an ion exchange chromatography afforded in good yields the desired free derivatives 11 and 12 (Figure 2), whose structure has been confirmed by proton and carbon NMR and by high-resolution mass spectra analysis.

Characterization of the glyconanotubes

The radical addition of aryl diazonium salts generated upon electrochemical or thermal treatment has shown to be a powerful tool by itself for the functionalization, solubilization, and

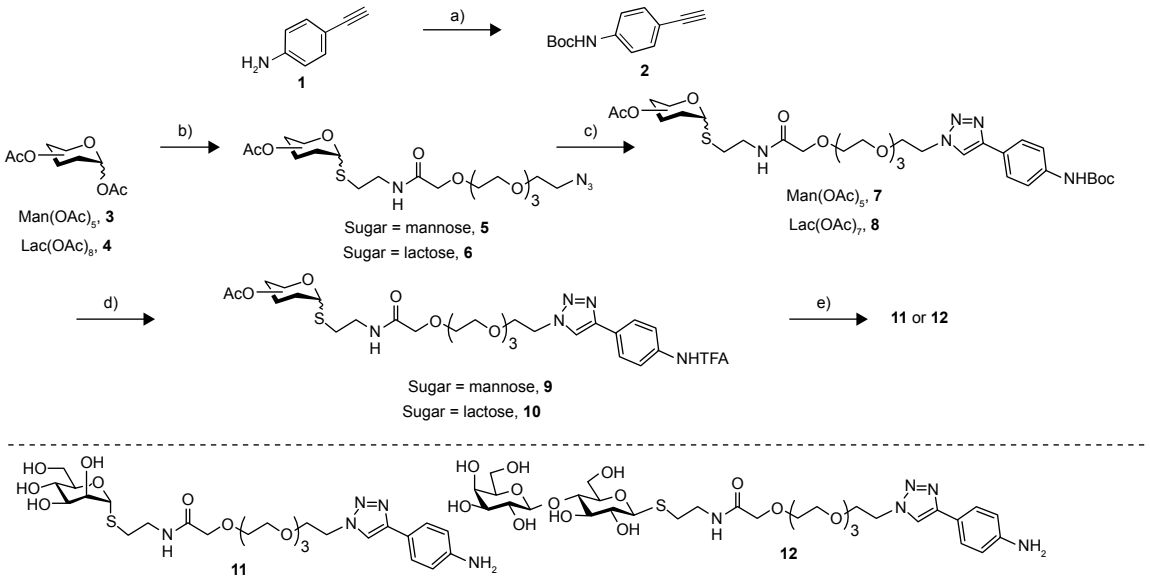

Figure 2 Synthetic pathway for the synthesis of derivatives 11 and 12.
Notes: (a) Boc_2O, THF, 54%; (b) see ref 36; (c) $CuSO_4$, sodium ascorbate, CH_2Cl_2/H_2O, MW, **7** (62%), **8** (80%); (d) TFA, CH_2Cl_2, **9** (99%), **10** (80%); (e) MeONa/MeOH, **11** (79%), **12** (60%).
Abbreviations: THF, tetrahydrofuran; MW, microwave; TFA, trifluoroacetic acid.

dispersion of SWCNTs.[48–50] In our examples, this reaction has shown to be an easy-to-perform and efficient approximation to afford the highly functionalized water-soluble carbon derivatives I and II. Specifically, a well-dispersed mixture of the corresponding aminophenyl derivative (11 or 12) and SWCNTs in a oDCB/DMF mixture was reacted with amyl nitrite at 65°C, affording, after the typical work-up, the title compounds (Figure 3).

The obtained derivatives I and II were fairly soluble in water at maximal concentration values of 0.25 and 0.28 g/L, respectively (Table 1), resulting in dark black solutions where neither depletion of the solute nor precipitation was observed after several weeks. The solubility trend follows both the functionalization degree and the solubility in water of the corresponding sugar by itself.[51] Moreover, both derivatives were also highly soluble in DMF at similar concentration values and stabilities than those of the aqueous solutions. On the contrary, the nanoconstructs were insoluble in MeOH and practically insoluble in THF or CH_3CN.

First, spectroscopies were used to corroborate qualitatively the covalent functionalization of SWCNTs. In this regard, UV/Vis/NIR spectra of adducts I and II in water or DMF (Figure 4A) exhibited an almost loss of the Van Hove singularities (even more pronounced in I), which is characteristic of the disrupted π system upon covalent functionalization. Moreover, Raman spectroscopy (Figure 4B) showed an increased D-band (dispersive disorder-induced mode) at ~1,300 cm^{-1} in regards with the G-band (tangential mode) at ~1,580 cm^{-1} compared to pristine SWCNTs. The ratio between the D-band and G-band intensities (I_D/I_G) is a good indicator of the quality of bulk samples and thus the degree of structural defects (hybridized sp^2 carbons to sp^3 due to covalent functionalization).[52] Indeed, the more similar this quotient is to unity, the higher is the introduction of

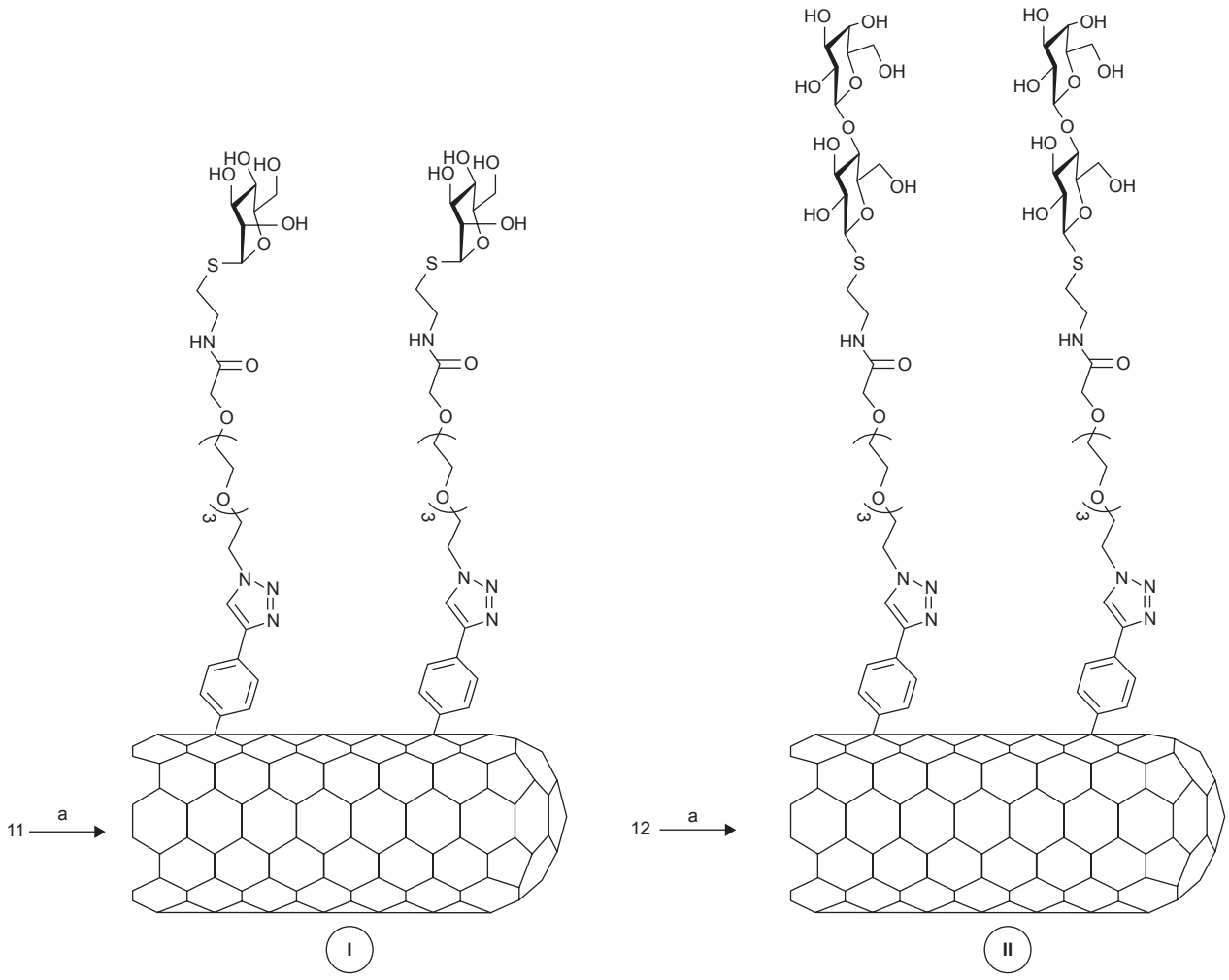

Figure 3 Synthetic pathway of derivatives I and II.
Notes: a refers to I: P2-SWCNT, oDCB/DMF; II: amyl nitrite, 65°C, 24 hours.
Abbreviations: SWCNT, single-walled carbon nanotube; oDCB, orthodichlorobenzene; DMF, dimethylformamide.

Table 1 Results on solubility/functionalization of derivatives glyconanotubes I and II

Entry	Material	Max solubility in water (g/L)	Sugar content (%)[a]	Sugar content (mmol/g)	I_D/I_G
1	Pristine SWCNTs	Negligible	0	0	0.08
2	I	0.25	42	0.68	0.22
3	II	0.28	63	0.8	0.27

Note: [a]Determined by TGA analyses.
Abbreviations: TGA, thermogravimetric analysis; SWCNT, single-walled carbon nanotube; I_D, D-band intensity; I_G, G-band intensity; Max, maximum.

functional groups covalently bound to the nanotube sidewall. Values of I_D/I_G equal to 0.22 and 0.27 were obtained for I and II, respectively, which is in good agreement with the solubility results mentioned earlier and therefore with the functionalization degree (Table 1).

Sugar-coated SWCNTs I and II were characterized by TEM, STEM, SEM, TGA, and Raman and UV/Vis/NIR spectroscopies. First, the morphology and dispersability of the prepared sugar-coated nanomaterials I and II in water solutions were investigated by TEM and STEM. Deposits of stock solutions thereof on a carbon-based TEM grid or STEM showed very low aggregated structures (Figure 5A–D) in comparison with the parent unfunctionalized carbon nanotubes. This fact supports the chemical functionalization and thus the debundling effect. Addition of a contrast agent (typically, 2% uranyl acetate in water)[53] was not necessary in order to obtain good-quality images of the dispersed aggregates.

The aggregates were further characterized by SEM. As in the case of TEM and STEM analyses, it is possible to observe the aggregates by simple deposition on SEM grids, we also analyzed metal-coated aggregates. For this purpose, after deposition of stock solutions on silicon wafer and drying, the samples were coated with gold by ion sputtering deposition. As with TEM and STEM analysis, dispersed nanoconstructs consisting mainly of isolated nanotubes or small bundles were observed (Figure 5E and F), further supporting the change of the electronic nature of the SWCNTs sidewall. The results gathered from the water dispersability, TEM, STEM, and SEM analyses clearly indicate that the sidewalls of the nanotubes are no more hydrophobic but are hydrophilic exposing the functional sugars to the water phase.

The quantification of sugar load on the SWCNTs was determined by TGA analysis. In the case of short-chain sugar-coated SWCNTs (Figure 6A and B), TGA analysis (20°C/min to 600°C, N_2) of I and II resulted in maximal weight loss of 25% and 35%, respectively, at 600°C. In comparison, at the same temperature, the starting carbohydrate derivatives 11 and 12 resulted in 62% weight losses. Then, by correlating these values, we estimated that the complete destruction of both monosaccharide 11 and disaccharide 12 within the aggregates I and II would cause mass losses at around 42% and 62%, respectively. This results prove that the degree of functionalization of nanosystem I is 42% (wt%), which means that for 1 g of the nanosystem I, there is 420 mg of deaminated mannose derivative 11, which corresponds to 0.68 mmol of mannoside derivative per gram of nanomaterial. In the same way for the nanosystem II, with a functionalization degree of 62%, for 1 g of nanosystem II, there is 620 mg of deaminated 12, which corresponds to 0.8 mmol of sugar derivative for each gram of nanomaterial.

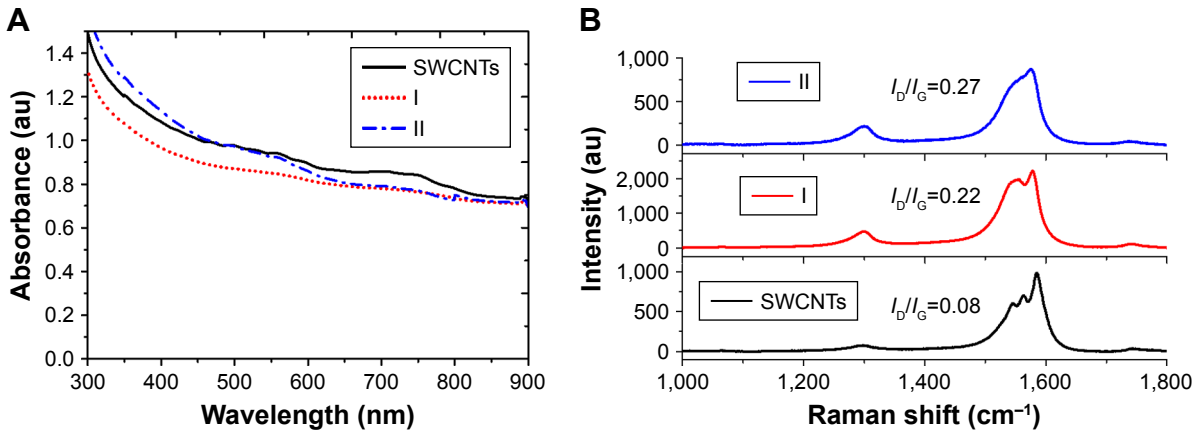

Figure 4 (**A**) UV/Vis/NIR spectra of long chain sugar-coated SWCNTs: SWCNTs (solid), I (red dotted line) and II (blue dashed line). (**B**) Comparative Raman spectra of SWCNTs (black), I (red), and II (blue) using a laser operating at 785 nm.
Abbreviations: UV/Vis/NIR, ultraviolet/visible/near infrared; SWCNTs, single-walled carbon nanotubes; I_D, D-band intensity; I_G, G-band intensity.

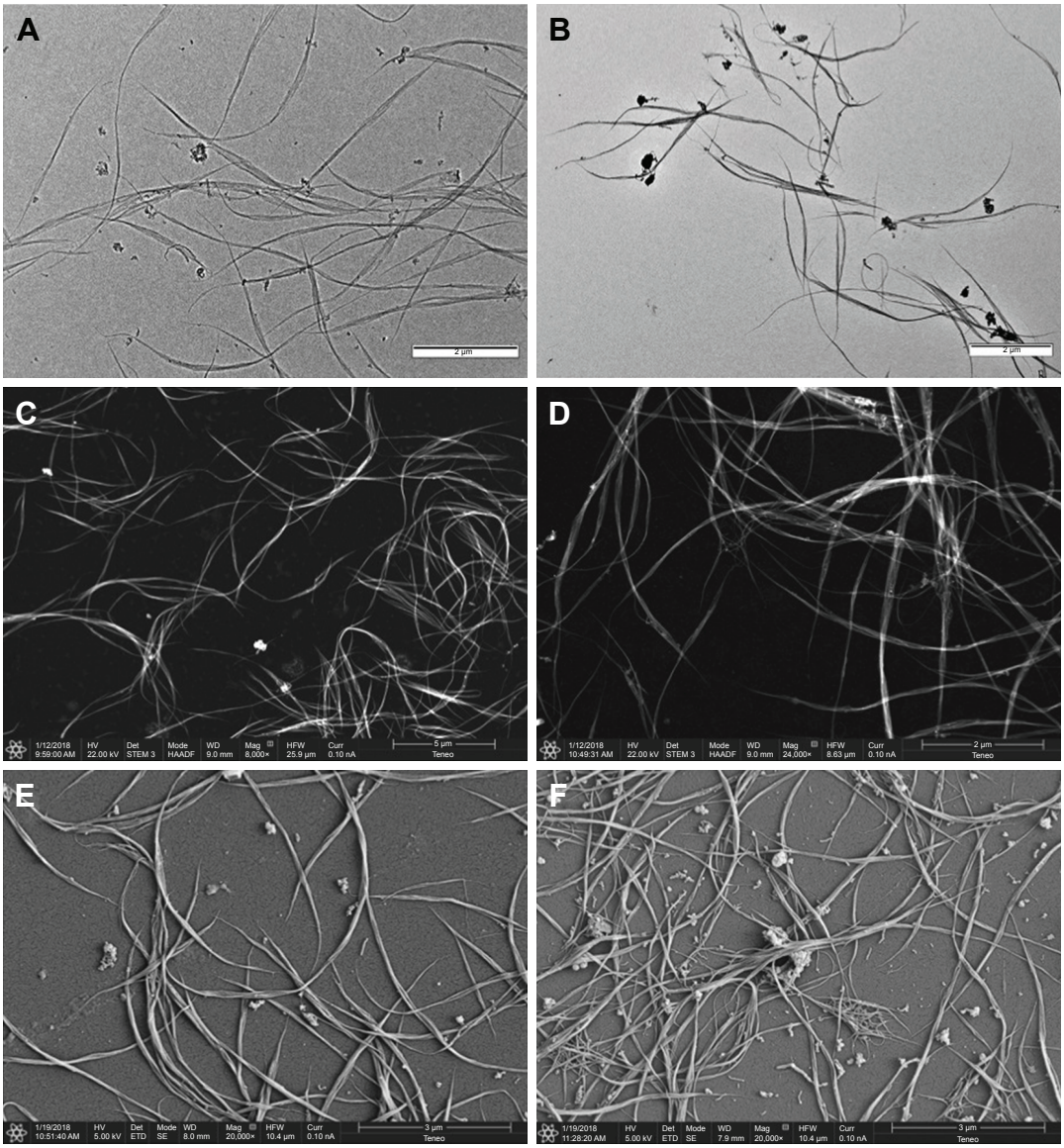

Figure 5 (**A**) TEM micrograph of water solutions of mannose-coated SWCNT I, (**B**) TEM micrograph of water solutions of lactose-coated SWCNT II, (**C**) STEM micrograph of water solutions of mannose-coated SWCNT I with HAADF detector, (**D**) STEM micrograph of water solutions of lactose-coated SWCNT II with HAADF detector, (**E**) SEM micrograph of water solutions of mannose-coated SWCNT I, and (**F**) SEM micrograph of water solutions of lactose-coated SWCNT II.
Abbreviations: TEM, transmission electronic microscopy; SWCNT, single-walled carbon nanotube; STEM, scanning transmission electronic microscopy; HAADF, high-angle darkfield; SEM, scanning electronic microscopy.

Selective agglutination of *E. coli* type 1 fimbriae studies

As stated in the introduction, the mannose-specific lectin FimH located at the tip of bacterial type 1 pili mediate the adhesion to the mannose moieties of glycosylated cell wall proteins.[54] As such, FimH constitute an appealing target for the development of mannose-based antagonist as new anti-adhesive drugs for preventing and treating UTIs. Therefore, we were interested in examining the ability of our glyconanosystems I and II to recognize and specifically aggregate bacteria, thereby preventing their attachment to cells of the urinary tract (Figure 7).

For that purpose, *E. coli* strains ORN178 (forming α-mannose interacting type 1 pili) and ORN208 (lacking the mannose receptor FimH)[55] were first transformed with the red fluorescent mCherry-protein expressing plasmid pGEM-T. *E. coli*–glyconanotube interactions were then followed by fluorescence microscopy. To avoid unspecific interaction with the growth medium, exponentially grown *E. coli* were diluted in Milli-Q water (Figure 8A–D), prior to a 30-minute incubation period in the presence of glyconanotubes I and II. Mannose-coated compounds I induced the formation *E. coli-I* clusters upon incubation with FimH-presenting

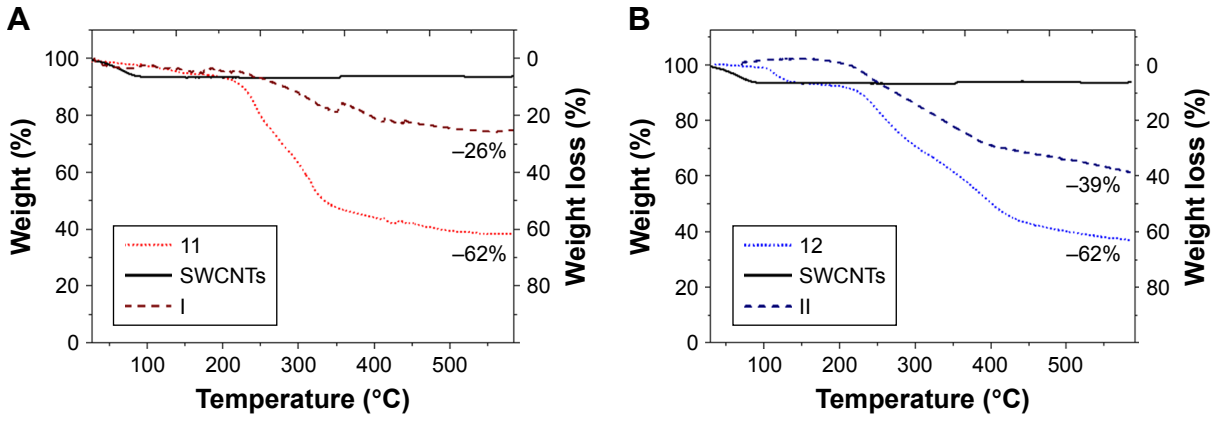

Figure 6 Thermograms by TGA of (**A**) mannose-coated SWCNT I (red) and (**B**) lactose-coated SWCNT II (blue), wherein compared the weight loss of the unfunctionalized SWCNTs (solid line), the starting carbohydrates (dotted), and the title compounds (dashed).
Abbreviations: TGA, thermogravimetric analysis; SWCNT, single-walled carbon nanotube.

ORN178 bacteria (Figure 8E and F), but not in the case of the FimH-devoid ORN208 strain (Figure 8G and H). Consequently lactose-coated nanomaterials II, do not induce the formation of *E. coli* aggregates (Figure 8I and J). Taken together, these results suggest that: 1) the aggregation process is specific and relies in the FimH–mannose interaction, and 2) the agglutination of bacterial cells may be favored by the presence of the PEG chain, thanks to its flexibility which would facilitate the positioning of the mannose ligand for better interaction with FimH lectin. Taken together these results suggest that: i) the aggregation process is specific, and relies in the FimH-mannose interaction, and ii) the agglutination of bacterial cells may be favored by the presence of the PEG chain, which thanks to its flexibility would facilitate the positioning of the mannose ligand for better interaction with FimH lectin (see more details in Figure S5 and Table S1).

In the case of the Man-SWCNTs I, the interaction of the exposed mannose residues with FimH receptors on the bacterial surface seemed to be extremely efficient at clustering *E. coli* in the form of a "fireball" formed by thousands of bacteria. The interaction of I with *E. coli* was further characterized by high-resolution TEM and SEM analyses (Figure 9). Negatively stained TEM image permits a closer look at ORN178-I and ORN178-II aggregates. In the former case, the bacteria were entangled by the mannose-coated nanotubes in a spider web-like morphology (Figure 9E). In contrast, ORN208 did not interact with mannose-coated nanotubes I, and these bacteria remained dispersed. Negative control experiments using lactose-coated nanotube Lac-SWCNTs II that is not a ligand of FimH, instead of II showed no formation of bacteria aggregates with ORN178. Sputter coat SEM analysis is an excellent method for the characterization of microbial morphology and for the diagnosis of infectious diseases. We therefore decided to characterize the bacterial–glyconanotube interactions by this technique, and the results obtained are shown in Figure 9 (see also Figure S6 and S7). In the case of the glyconanotubes I exposing the mannose sugar to the aqueous phase, the image shows the formation of a bacteria aggregate in the form of a brick wall cemented by the glyconanotubes.

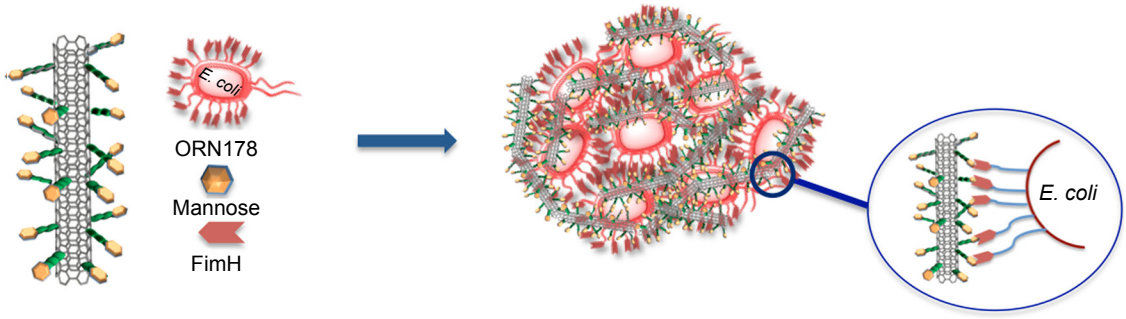

Figure 7 Schematic representation of the FimH adhesin promoted specific interaction of *E. coli* with mannose-coated SWCNTs I.
Abbreviations: SWCNTs, single-walled carbon nanotubes; *E. coli*, *Escherichia coli.*

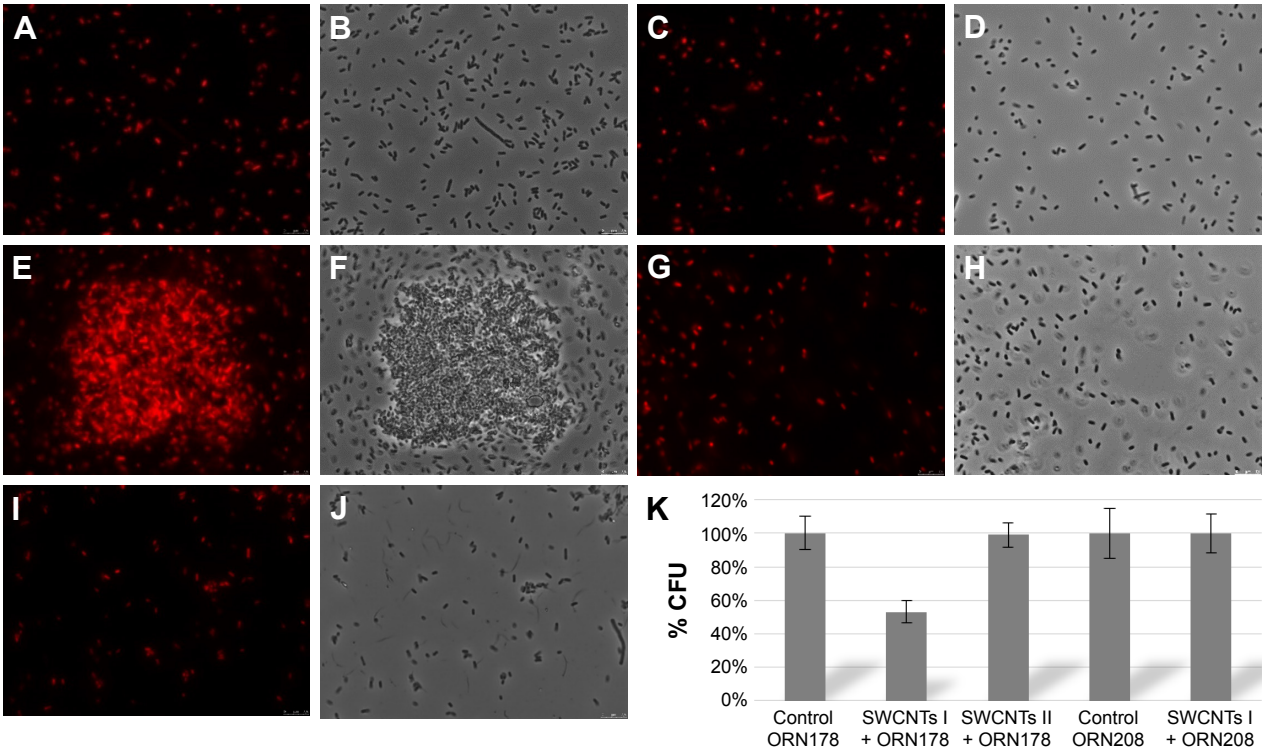

Figure 8 Representative fluorescence microscopy images of the interaction of glyconanotubes I and II with *E. coli* strain ORN178 and ORN208.
Notes: (**A**, **B**) *E. coli* strain ORN178 alone. (**C**, **D**) *E. coli* strain ORN208 alone. (**E**, **F**) Selective interaction of glyconanotube I with the *E. coli* strain ORN178. (**G**, **H**) Interaction of glyconanotube I with the *E. coli* strain ORN208. (**I**, **J**) Interaction of glyconanotube II with the *E. coli* strain ORN178. (**K**) CFU assay (see Figure S5 and Table S1 for more information). The number of colonies formed in the absence (control) and presence of glyconanotube I for ORN178 and ORN208 cells is indicated. For conditions, see "Materials and methods" section in the text.
Abbreviations: SWCNTs, single-walled carbon nanotubes; *E. coli*, *Escherichia coli*; CFU, colony-forming unit.

On the contrary, both in the case of the incubation of glyconanotube I with bacterial strain ORN208, and in the case of the incubation of lactose-coated SWCNTs II with bacterial strain ORN178 having the lectin FimH, the bacteria remain dispersed and establish no interaction with the nanotubes, which is perfectly visible on the image. These results further support the idea that glyconanotubes I bind to bacteria through a selective mannose–FimH receptor interaction.

Uncontrolled bacterial proliferation is an important threat to human health leading to inflammation and activation of the immune system. The adhesion of uropathogenic, fimbriated bacteria to the mannose moieties of glycosylated cell wall proteins is well studied. Type 1 fimbriae are adherence factors encoded by the chromosomally located fim gene cluster (FimA-FimH) in *E. coli*, and FimH recognizes terminally located D-mannose moieties on cell-bound and secreted glycoproteins. Imitating this multivalent system (SWCNTs I), we could agglutinate them and inhibit their capacity of infection.[56–60] For that reason, in order to prove, with a quantitative idea, the interaction of the aggregation between *E. coli* type 1 fimbriae and functionalized SWCNTs with mannose, a reduction test of the CFU has been carried out. The first step was the incubation of *E. coli* strains ORN178 (forming α-mannose interacting type 1 pili) and ORN208 (lacking the mannose receptor FimH) with compound I (SWCNTs-PEG-Man) and compound II (SWCNTs-PEG-Lac) and then centrifuge with a low speed that selectively leads to the precipitation of bacteria–SWCNTs aggregates. Bacteria that remained in the supernatant were then seeded on LB plates and incubated overnight to allow colony formation. The results obtained are shown in Figure 8K (Figure S5 and Table S1), where on one hand no effect with SWCNTs II is observed; however, on the other hand, with SWCNTs I, a considerable reduction of the CFU is appreciated (around 50%), in comparison with the control, due to the important coating of the carbon nanotubes with the mannose derivatives and their strong interaction with *E. coli* ORN178. Moreover, in the case of *E. coli* ORN208 there was no reduction of the CFU, confirming the high specificity of the interaction between the aggregates and *E. coli* ORN178. We hypothesize that the tetraethylene glycol spacer in SWCNTs I nanomaterial

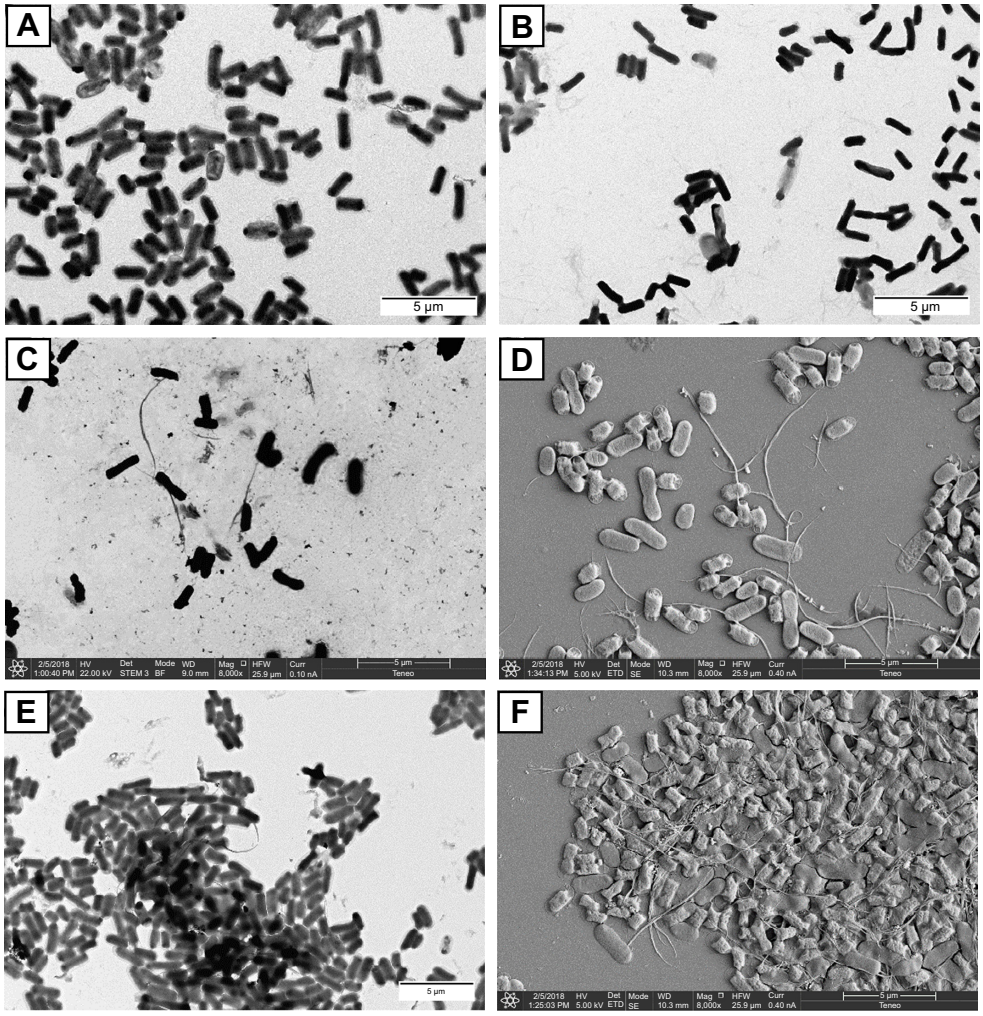

Figure 9 Representative, negatively stained TEM and sputter coated with gold, micrographs of the interaction of glyconanotubes I and II with *E. coli* strains ORN178 and ORN208.
Notes: (**A**) TEM micrograph of *E. coli* strain ORN178 alone. (**B**) TEM micrograph of *E. coli* strain ORN208 alone. (**C**) TEM micrograph of the lactose-coated glyconanotube II incubated with the *E. coli* strain ORN178. (**D**) SEM micrograph of sputter coated with gold of glyconanotube II incubated with *E. coli* strain ORN178. (**E**) TEM micrograph of the mannose-coated glyconanotube I incubated with the *E. coli* strain ORN178. (**F**) SEM micrograph of sputter coated with gold of glyconanotube I incubated with *E. coli* strain ORN178. For conditions, see "Materials and methods" section in the text. Size bars are shown.
Abbreviations: TEM, transmission electronic microscopy; SWCNTs, single-walled carbon nanotubes; *E. coli*, *Escherichia coli*; SEM, scanning electronic microscopy.

improves the adaptability of the sugar mannose for a better interaction with the adhesin FimH of the bacteria.

Conclusion

In conclusion, we have demonstrated the suitability of the radical addition reaction of aminophenyl-substituted sugars to achieve elevated covalent functionalization of SWCNTs and to modulate their surface. The methodology, simple to implement experimentally, provides robust aggregates, highly dispersed in water and exposing a large number of sugars to the aqueous phase. The two 1D aggregates obtained with a multivalent exposure of mannose and lactose on their surface were tested as selective adhesives and selective inhibitors of bacterial cell growth. This in vivo study showed that unlike nano-object II, exposing lactose, nano-object I, exposing mannose on the nanotube surface, is able to agglutinate bacteria. The reported results constitute additional data in favor of using mannose-coated 1D carbon nanotubes as antiadhesive drugs that compete for FimH binding and prevent the uropathogenic bacteria from adhering to the urothelial surface.

Acknowledgments

Financial support was provided by the PAIDI Program of the Andalusian Government (FQM-313 to NK, BIO-026 to REW), and the Spanish Ministry of Economy and Competitiveness

(CTQ2016-78580-C2-1-R to NK) the University of Seville (V PLAN PROPIO to REW). The European Regional Development Fund (FEDER) and the European Social Fund (ESF) are also acknowledged. We thank the Center of Research Technology and Innovation of the University of Seville (CITIUS) for the use of TEM, AFM, and NMR facilities. Mohyeddin Assali current adress: Department of Pharmacy, Faculty of Medicine and Health Science, An Najah National University.

Disclosure

ERB is recipient of an FPU PhD fellowship from the Spanish Ministry of Education, Culture and Sport. EF is recipient of a fellowship from the Junta de Andalucia (P11-CTS-7962/FEDER). The authors report no other conflicts of interest in this work.

References

1. Mammen M, Choi SK, Whitesides GM. Polyvalent interactions in biological systems: implications for design and use of multivalent ligands and inhibitors. *Angew Chem Int Ed*. 1998;37:2754–2794.
2. Fasting CA, Schalley M, Weber O, et al. Multivalency as a chemical organization and action principle. *Angew Chem Int Ed*. 2012;51:2754–2794.
3. Mulder A, Huskens J, Reinhoudt DN. Multivalency in supramolecular chemistry and nanofabrication. *Org Biomol Chem*. 2004;2(23):3409–3424.
4. Lee RT, Lee YC. Affinity enhancement by multivalent lectin-carbohydrate interaction. *Glycoconj J*. 2000;17(7–9):543–551.
5. Sacchettini JC, Baum LG, Brewer CF. Multivalent protein-carbohydrate interactions. A new paradigm for supermolecular assembly and signal transduction. *Biochemistry*. 2001;40(10):3009–3015.
6. Brewer CF, Miceli MC, Baum LG. Clusters, bundles, arrays and lattices: novel mechanisms for lectin-saccharide-mediated cellular interactions. *Curr Opin Struct Biol*. 2002;12(5):616–623.
7. Lundquist JJ, Toone EJ. The cluster glycoside effect. *Chem Rev*. 2002;102(2):555–578.
8. Pieters RJ. Maximising multivalency effects in protein-carbohydrate interactions. *Org Biomol Chem*. 2009;7(10):2013–2025.
9. Becer CR. The glycopolymer code: synthesis of glycopolymers and multivalent carbohydrate-lectin interactions. *Macromol Rapid Commun*. 2012;33(9):742–752.
10. Werz DB, Seeberger PH. Carbohydrates as the next frontier in pharmaceutical research. *Chemistry*. 2005;11(11):3194–3206.
11. Bhatia S, Dimde M, Haag R. Multivalent glycoconjugates as vaccines and potential drug candidates. *Med Chem Commun*. 2014;5(7):862–878.
12. Astronomo RD, Burton DR. Carbohydrate vaccines: developing sweet solutions to sticky situations? *Nat Rev Drug Discov*. 2010;9(4):308–324.
13. Hudak JE, Bertozzi CR. Glycotherapy: new advances inspire a reemergence of glycans in medicine. *Chem Biol*. 2014;21(1):16–37.
14. Johnson KF. Synthesis of oligosaccharides by bacterial enzymes. *Glycoconj J*. 1999;16(2):141–146.
15. Foxman B, Barlow R, D'Arcy H, Gillespie B, Sobel JD, D'Arcy H. Urinary tract infection: self-reported incidence and associated costs. *Ann Epidemiol*. 2000;10(8):509–515.
16. World Health Organization. *Antibiotic Resistance: Multi-Country Public Awareness Survey*. Geneva: World Health Organization; 2015:512.
17. Czaplewski L, Bax R, Clokie M, et al. Alternatives to antibiotics: a pipeline portfolio review. *Lancet Infect Dis*. 2016;16(2):239–251.
18. Payne DJ, Gwynn MN, Holmes DJ, Pompliano DL. Drugs for bad bugs: confronting the challenges of antibacterial discovery. *Nat Rev Drug Discov*. 2007;6(1):29–40.
19. Tommasi R, Brown DG, Walkup GK, Manchester JI, Miller AA. ESKAPEing the labyrinth of antibacterial discovery. *Nat Rev Drug Discov*. 2015;14(8):529–542.
20. Gill EE, Franco OL, Hancock RE. Antibiotic adjuvants: diverse strategies for controlling drug-resistant pathogens. *Chem Biol Drug Des*. 2015;85(1):56–78.
21. Jones CH, Pinkner JS, Roth R, et al. FimH adhesin of type 1 pili is assembled into a fibrillar tip structure in the Enterobacteriaceae. *Proc Natl Acad Sci U S A*. 1995;92(6):2081–2085.
22. Mayer K, Eris D, Schwardt O, et al. Urinary tract infection: which conformation of the bacterial lectin FimH is therapeutically relevant? *J Med Chem*. 2017;60(13):5646–5662.
23. Sharon N. Carbohydrates as future anti-adhesion drugs for infectious diseases. *Biochimica et Biophysica Acta (BBA) – General Subjects*. 2006;1760(4):527–537.
24. Bernardi A, Jiménez-Barbero J, Casnati A, et al. Multivalent glycoconjugates as anti-pathogenic agents. *Chem Soc Rev*. 2013;42(11):4709–4727.
25. Kang B, Opatz T, Landfester K, Wurm FR. Carbohydrate nanocarriers in biomedical applications: functionalization and construction. *Chem Soc Rev*. 2015;44(22):8301–8325.
26. Dosekova E, Filip J, Bertok T, Both P, Kasak P, Tkac J. Nanotechnology in glycomics: applications in diagnostics, therapy, imaging, and separation processes. *Med Res Rev*. 2017;37(3):514–626.
27. Ryu JH, Lee E, Lim YB, Lee M, Lim YB. Carbohydrate-coated supramolecular structures: transformation of nanofibers into spherical micelles triggered by guest encapsulation. *J Am Chem Soc*. 2007;129(15):4808–4814.
28. Lim Y-B, Park S, Lee E. Tunable bacterial agglutination and motility inhibition by self-assembled glyco-nanoribbons. *Chemistry*. 2007;2(11):1363–1369.
29. Dane EL, Ballok AE, O'Toole GA, Grinstaff MW. Synthesis of bio-inspired carbohydrate amphiphiles that promote and inhibit biofilms. *Chem Sci*. 2014;5(2):551–557.
30. Cid JJ, Assali M, Fernández E. Tuning glyconanomaterials size and shape for selective bacterial cell agglutination. *J Mat Chem B*. 2016;4:2028–2037.
31. Fabbro C, Ali-Boucetta H, da Ros T, Kostarelos K, Bianco A, Prato M. Targeting carbon nanotubes against cancer. *Chem Commun*. 2012;48(33):3911–3926.
32. Li Z, Branco de Barros AL, Ferreira Soares DC, et al. Functionalized single-walled carbon nanotubes: cellular uptake, biodistribution and applications in drug delivery. *Int J Pharm*. 2017;524:41–54.
33. Khiar N, Leal MP, Baati R, et al. Tailoring carbon nanotube surfaces with glyconanorings: new bionanomaterials with specific lectin affinity. *Chem Commun*. 2009;126(27):4121–4123.
34. Assali M, Leal MP, Fernández I, Baati R, Mioskowski C, Khiar N. Non-covalent functionalization of carbon nanotubes with glycolipids: glyconanomaterials with specific lectin-affinity. *Soft Matter*. 2009;5(5):948–950.
35. Assali M, Leal MP, Fernández I, Romero-Gomez P, Baati R, Khiar N. Improved non-covalent biofunctionalization of multi-walled carbon nanotubes using carbohydrate amphiphiles with a butterfly-like polyaromatic tail. *Nano Res*. 2010;3(11):764–778.
36. Pernía Leal M, Assali M, Cid JJ, et al. Synthesis of 1D-glyconanomaterials by a hybrid noncovalent-covalent functionalization of single wall carbon nanotubes: a study of their selective interactions with lectins and with live cells. *Nanoscale*. 2015;7(45):19259–19272.
37. Dyke CA, Tour JM. Unbundled and highly functionalized carbon nanotubes from aqueous reactions. *Nano Letters*. 2003;3(9):1215–1218.
38. Flatt AK, Chen B, Tour JM. Fabrication of carbon nanotube-molecule-silicon junctions. *J Am Chem Soc*. 2005;127:8918–8919.
39. Karousis N, Economopoulos SP, Iizumi Y, et al. Microwave assisted covalent functionalization of C(60)@SWCNT peapods. *Chem Commun*. 2010;46(48):9110–9112.
40. Peng X, Wong SS. Functional covalent functionalization of carbon nanotube surfaces. *Adv Mater*. 2009;21:625–642.
41. Karousis N, Tagmatarchis N, Tasis D. Current progress on the chemical modification of carbon nanotubes. *Chem Rev*. 2010;110:5366–5397.

42. Britz DA, Khlobystov AN. Noncovalent interactions of molecules with single walled carbon nanotubes. *Chem Soc Rev*. 2006;35(7):637–659.
43. Zhao YL, Stoddart JF. Noncovalent functionalization of single-walled carbon nanotubes. *Acc Chem Res*. 2009;42(8):1161–1171.
44. Lee Y, Geckeler KE. Carbon nanotubes in the biological interphase: the relevance of noncovalence. *Adv Mater*. 2010;22(36):4076–4083.
45. Gao Z, Varela JA, Groc L, Lounis B, Cognet L. Toward the suppression of cellular toxicity from single-walled carbon nanotubes. *Biomater Sci*. 2016;4(2):230–244.
46. Leal MP, Assali M, Fernández I, Khiar N. Copper-catalyzed azide-alkyne cycloaddition in the synthesis of Polydiacetylene: "Click Glycoliposome" as biosensors for the specific detection of lectins. *Chemistry*. 2011;17(6):1828–1836.
47. Jennifer R, Allen JR, Allen JG. *Chem Eur J*. 2000;6:1366–1375.
48. Dyke CA, Tour JM. Unbundled and highly functionalized carbon nanotubes from aqueous reactions. *Nano Letters*. 2003;3(9):1215–1218.
49. Flatt AK, Chen B, Tour JM. Fabrication of carbon nanotube-molecule-silicon junctions. *J Am Chem Soc*. 2005;127(25):8918–8919.
50. Mohamed AA, Salmi Z, Dahoumane SA, Mekki A, Carbonnier B, Chehimi MM. Functionalization of nanomaterials with aryldiazonium salts. *Adv Colloid Interface Sci*. 2015;225:16–36.
51. Gray MC, Converse AO, Wyman CE. Sugar monomer and oligomer solubility: data and predictions for application to biomass hydrolysis. *Appl Biochem Biotechnol*. 2003;105–108(1–3):179–194.
52. Graupner R. Raman spectroscopy of covalently functionalized single-wall carbon nanotubes. *J Raman Spectrosc*. 2007;38(6):673–683.
53. Richard C, Balavoine F, Schultz P, Moreau N, Mioskowski C. Immobilization of histidine-tagged proteins on functionalized carbon nanotubes. *J Bionanosci*. 2007;1(2):106–113.
54. Hartmann M, Lindhorst TK. The bacterial lectin FimH, a target for drug discovery-carbohydrate inhibitors of Type 1 fimbriae-mediated bacterial adhesion. *Eur J Org Chem*. 2011;(20–21):3583–3609.
55. Harris SL, Spears PA, Havell EA, Hamrick TS, Horton JR, Orndorff PE. Characterization of *Escherichia coli* type 1 pilus mutants with altered binding specificities. *J Bacteriol*. 2001;183(13):4099–4102.
56. Lim Y-B, Park S, Lee E. Tunable bacterial agglutination and motility inhibition by self-assembled glyco-nanoribbons. *Chemistry*. 2007;2(11):1363–1369.
57. Lim YB, Park S, Lee E, et al. Glycoconjugate nanoribbons from the self-assembly of carbohydrate-peptide block molecules for controllable bacterial cell cluster formation. *Biomacromolecules*. 2007;8(5):1404–1408.
58. Wang H, Gu L, Lin Y, et al. Unique aggregation of anthrax (*Bacillus anthracis*) spores by sugar-coated single-walled carbon nanotubes. *J Am Chem Soc*. 2006;128(41):13364–13365.
59. Luo PG, Wang H, Gu L, et al. Selective interactions of sugar-functionalized single-walled carbon nanotubes with *Bacillus* spores. *ACS Nano*. 2009;3(12):3909–3916.
60. Gu L, Elkin T, Jiang X, et al. Single-walled carbon nanotubes displaying multivalent ligands for capturing pathogens. *Chem Commun*. 2005;37(7):874–876.

Supplementary materials

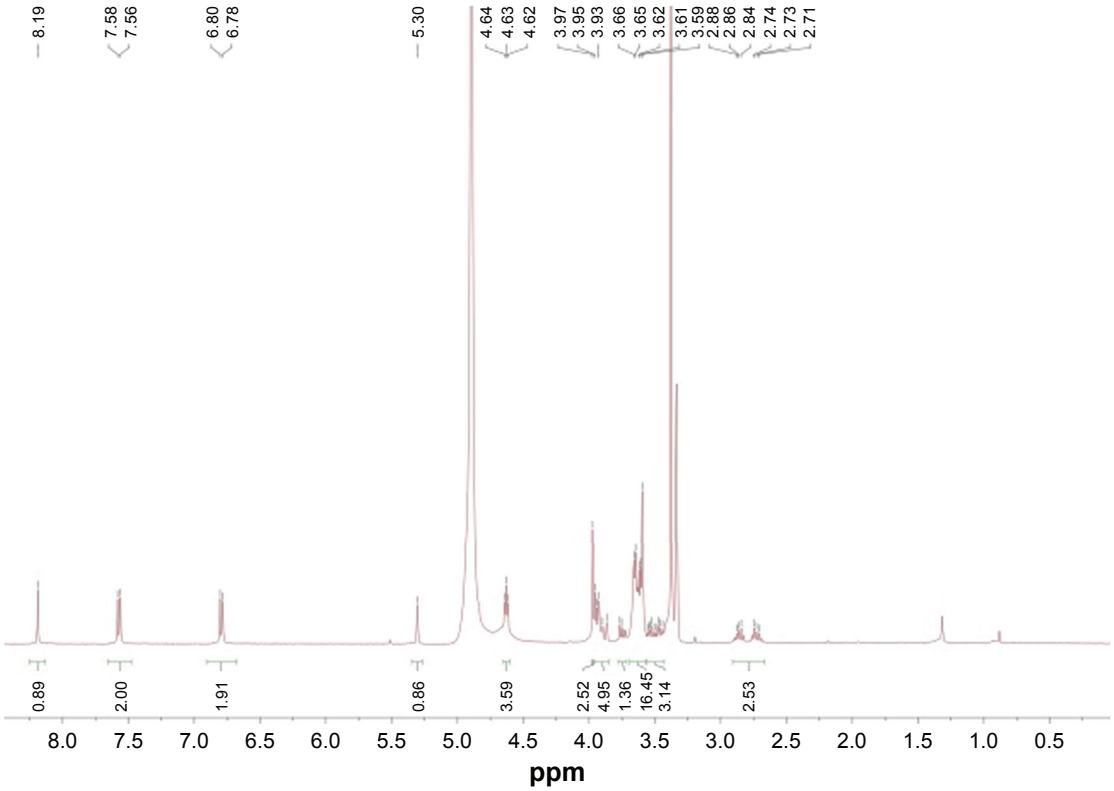

Figure S1 ^{1}H-NMR of final monomer **11**.
Abbreviation: NMR, nuclear magnetic resonance.

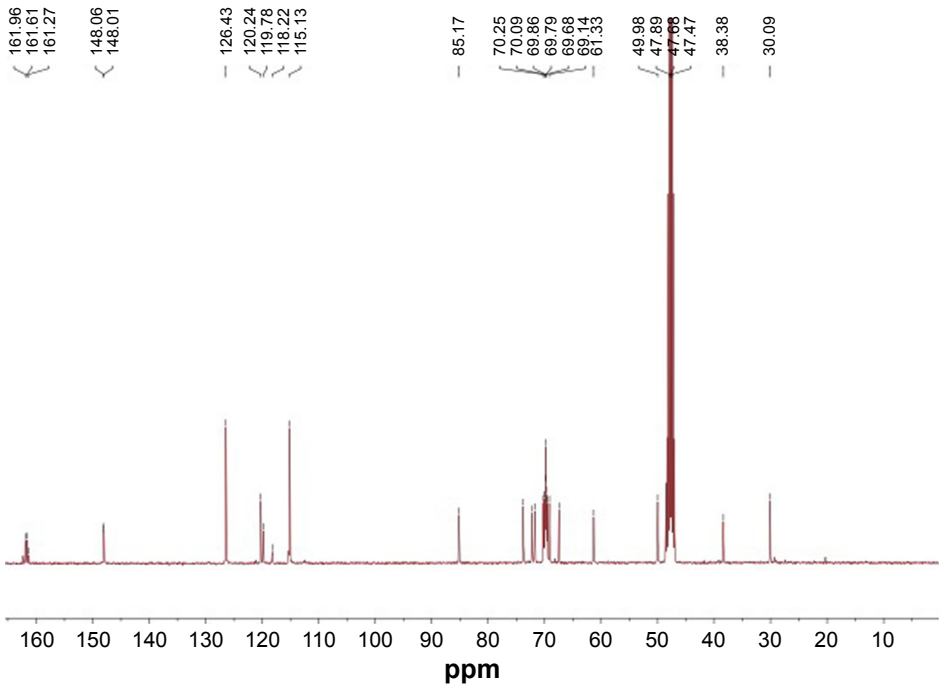

Figure S2 ^{13}C-NMR of final monomer **11**.
Abbreviation: NMR, nuclear magnetic resonance.

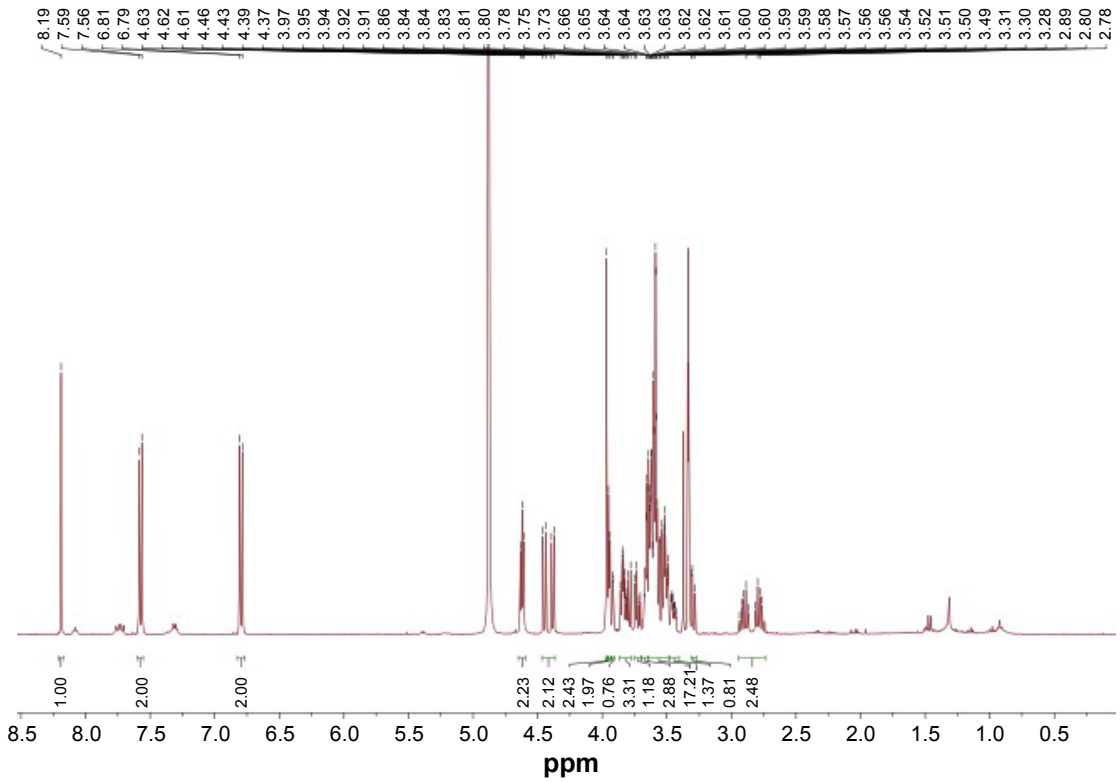

Figure S3 ^{1}H-NMR of final monomer **12**.
Abbreviation: NMR, nuclear magnetic resonance.

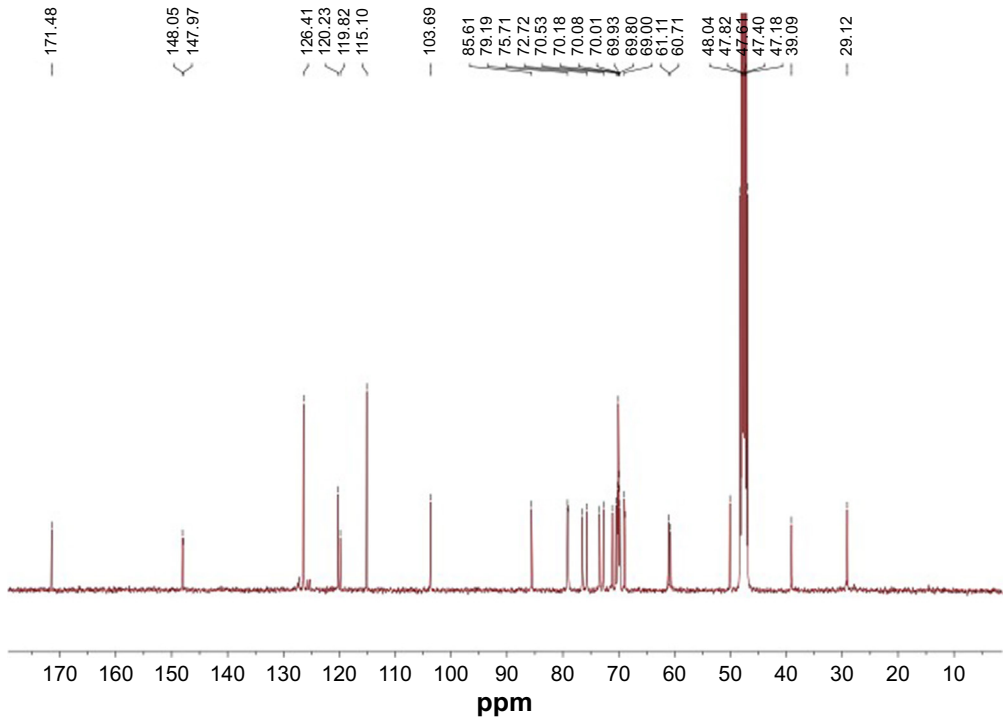

Figure S4 ^{13}C-NMR of final monomer **12**.
Abbreviation: NMR, nuclear magnetic resonance.

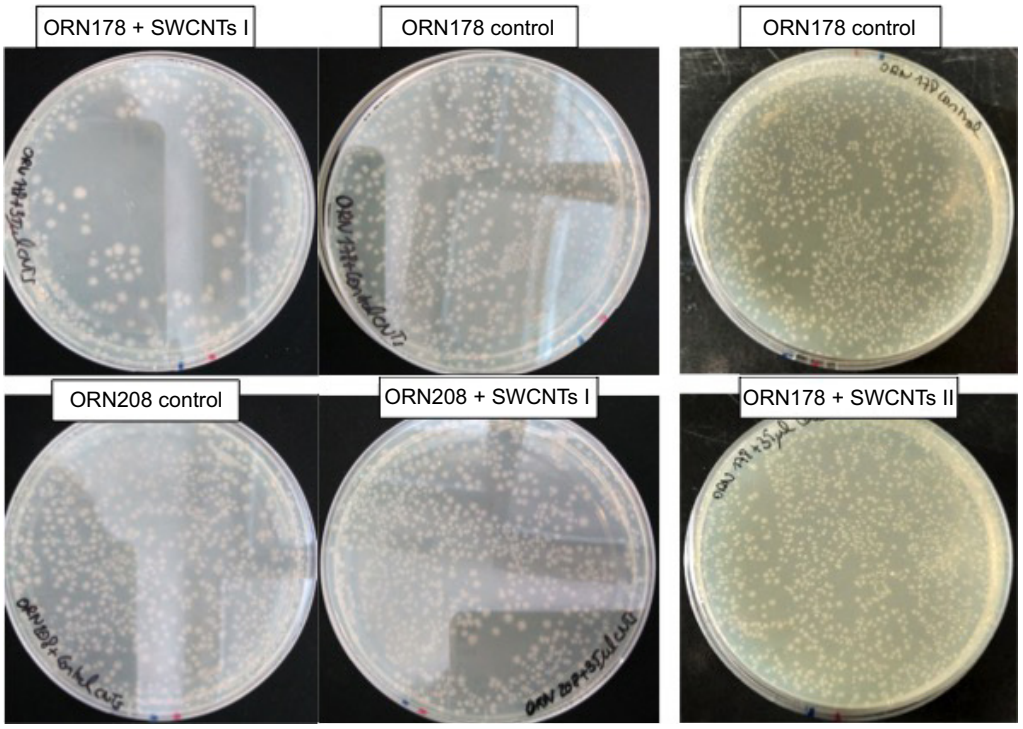

Figure S5 CFU reduction test of *E. coli* strains ORN178 and ORN208 with glyconanotubes I and II.
Abbreviations: CFU, colony forming units; *E. coli*, *Escherichia coli.*

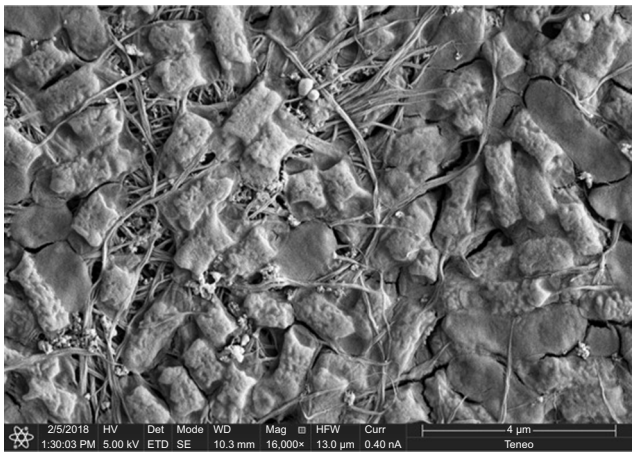

Figure S6 SEM image of bacterial agglutination by glyconanomaterial I.
Abbreviation: SEM, scanning electronic microscopy.

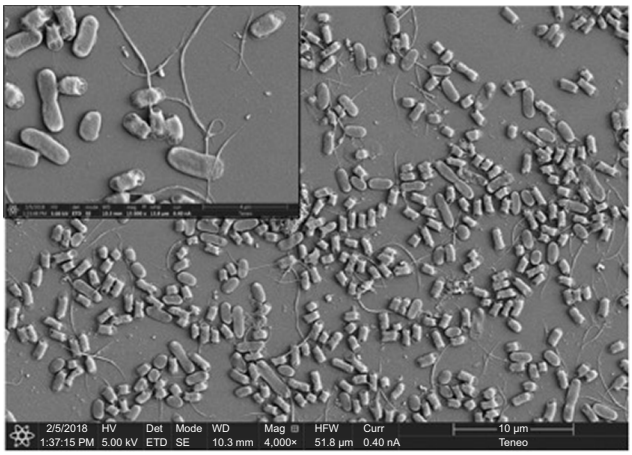

Figure S7 SEM image of no bacterial agglutination by glyconanomaterial II.
Abbreviation: SEM, scanning electronic microscopy.

Table S1 CFU reduction test of *E. coli* strains ORN178 and ORN208 with glyconanotubes I and II

CFU	Control ORN178	ORN178+ SWCNTs I	Control ORN208	ORN208+ SWCNTs I	Control ORN178	ORN178+ SWCNTs II
1	1,212	485	1,080	1,198	1,701	1,638
2	1,049	571	961	1,162	1,838	1,757
3	986	554	936	1,003	1,785	1,869
4	986	655	1,285	935	1,575	1,594
Average	1,066	566	1,056	1,074	1,725	1,714
SD	106.71	69.88	159.24	125.81	114.66	123.89
Average (%)	100%	53%	100%	100%	100%	99.4%
SD	10.01%	6.54%	15.08%	11.71%	6.64%	7.18%

Abbreviations: SWCNTs, single-walled carbon nanotubes; CFU, colony forming units; *E. coli*, *Escherichia coli*.